Supplement of Geosci. Model Dev., 18, 1737–1767, 2025
https://doi.org/10.5194/gmd-18-1737-2025-supplement

Geoscientific Model Development
Open Access
EGU

Supplement of

Long-term hydro-economic analysis tool for evaluating global groundwater cost and supply: Superwell v1.1

Hassan Niazi et al.

Correspondence to: Hassan Niazi (hassan.niazi@pnnl.gov)

S1 Geo-processed Hydrogeological Conditions

The World Hydrological Classification (WHY class) categorizes aquifers into classes that are easy (30), medium (10), or hard (20) for well installation, reflecting the aquifer's hydrocomplexity and directly influencing installation cost rates based on these classifications (Richts et al., 2011). These hydrogeological classifications/types of aquifers have a large bearing on the cost accounting, particularly impacting the well installation costs (Niazi et al., 2024c). We have used the aquifer classes and their HYGE property from WHYMAPs datasets from Richts et al., (2011) to determine the complexity, i.e., WHYMAP Class 10 as major groundwater basins, Class 20 as local and shallow aquifers and Class 30 as complex hydrogeological structures.

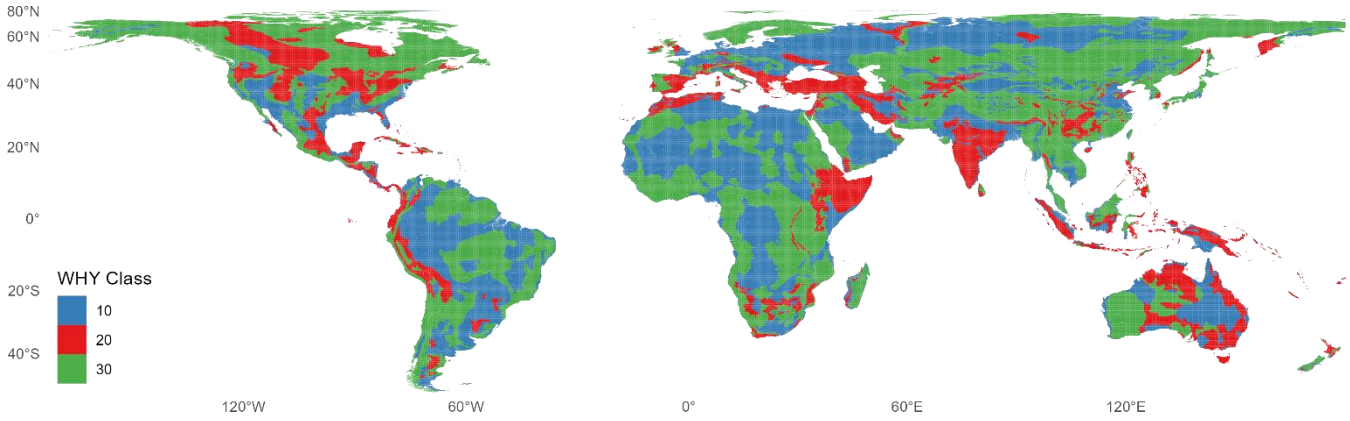

Fig. S1: WHYMap aquifer classes based on Richts et al., (2011)

Grid area shows intersections of spatial boundaries (countries, basins, WHY class) with rectilinear grid of 0.5 degree (roughly 50 km by 50 km) to keep homogeneous grid cells (Niazi et al., 2025).

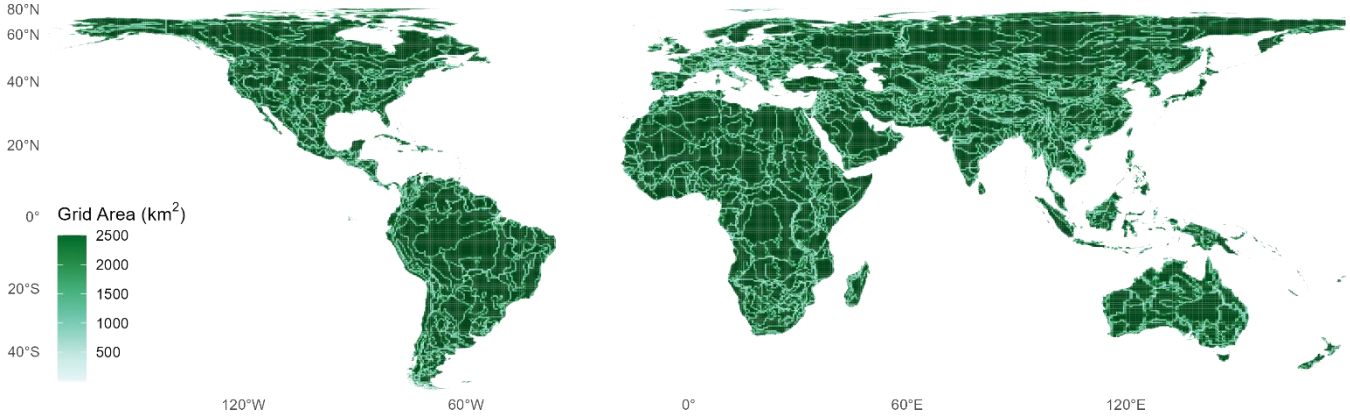

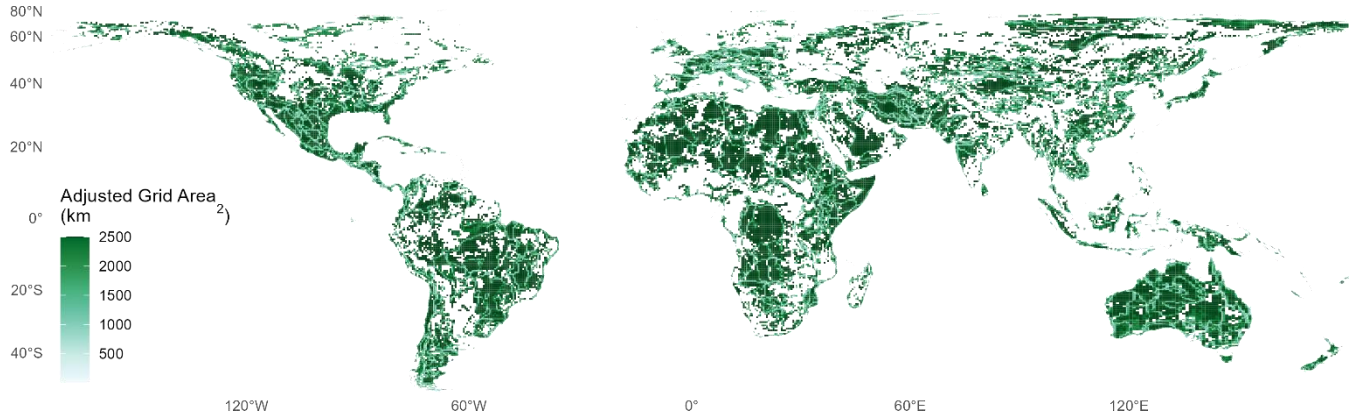

Fig. S2: Area of grid cells in km^2 discretized for superwell

Table S1: Descriptive statistics of geo-processed aquifer conditions across all grid cells globally (count = 106,432) used as input conditions for superwell

	Porosity (-)	Permeability (m^2)	Aquifer Thickness (m)	Depth to Water (m)	Grid Area (km^2)
Mean	0.138106	-13.765	329.8149	24.16211	1200.8
Standard Deviation	0.059178	0.796782	250.5558	22.40557	1028.4
Minimum	0.01	-16.5	37	0	0.0
1st Quartile (25%)	0.099375	-14.2286	200	7.222222	92.3
Median	0.141707	-13.7333	266.8706	17.22222	1045.3
3rd Quartile (75%)	0.19	-13.1714	376.2083	35.13571	2486.0
Maximum	0.28	-10.9	4665	196.5556	2500.7

S1.1 Limitations of Global Hydrogeological Datasets

Like all data, the global hydrogeological datasets used in this work have uncertainty and limitations embedded in them, including how well the global datasets capture aquifer properties (Niazi et al., 2024b). For example, the Fan et al. (2013) data used for depth to groundwater only provides global scale estimates of pre-development unconfined water depths. Similarly, the Gleeson et al. (2014) data porosity and permeability only provides estimates of the dominant surficial lithology (unconsolidated sediment, sedimentary rock, volcanic rock, etc.). Given the limitation of these datasets, it is not possible to resolve layered aquifer units because we lack the hydro-stratigraphy and accompanying water depth/confined aquifer head data to represent such systems. For regions that rely on deeper confined aquifers for the majority of their water supply, local scale studies and information would be more appropriate.

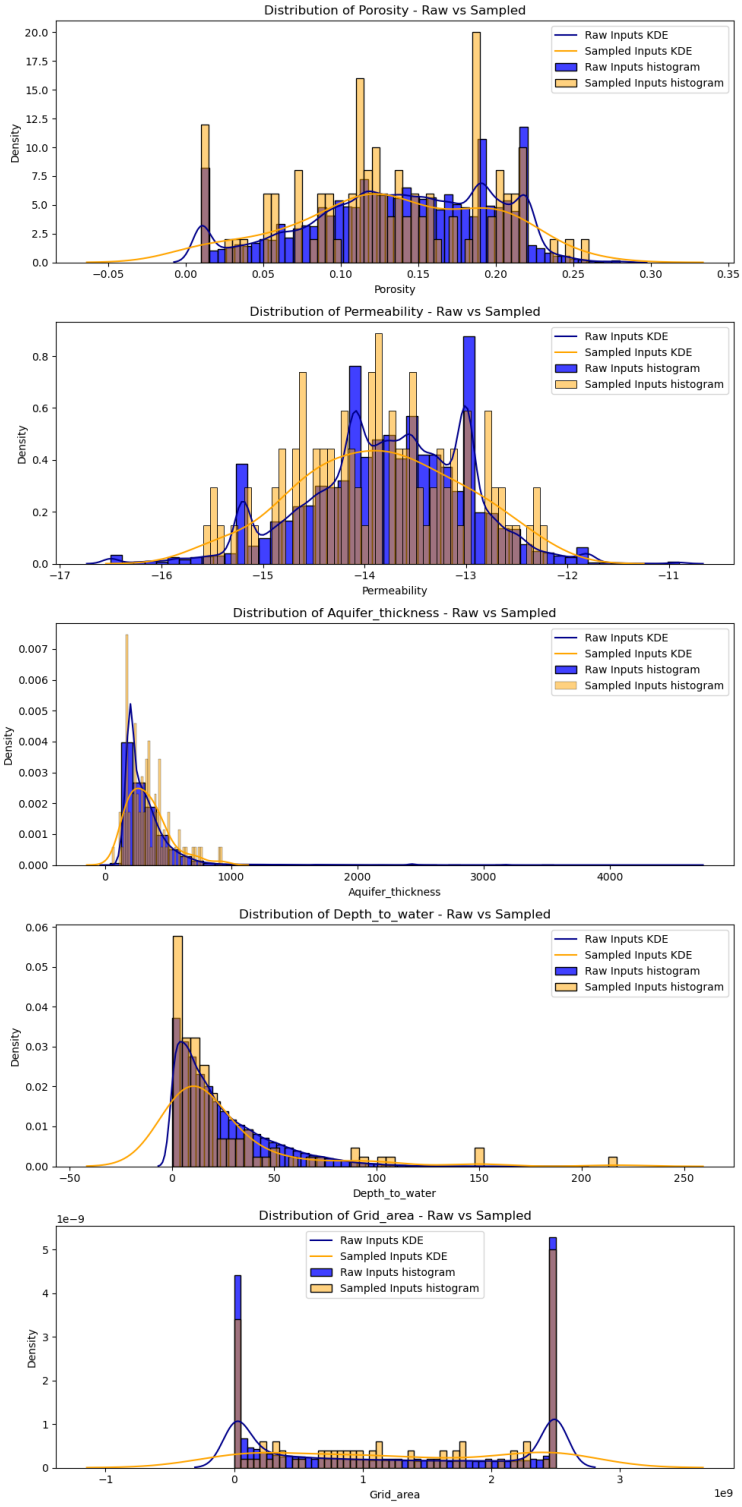

Fig. S3: Kernel density estimates of aquifer properties used as inputs to *Superwell*

S2 Dynamics for a Single Grid Cell

This example has been created to demonstrate Superwell dynamics using a single grid cell and a single scenario of moderate depletion (25%) and low ponded depth (0.3m) (without accounting for recharge related adjustments) (Niazi et al., 2024a; Niazi et al., 2024c). In this example, wells are deepened in year 16 (Fig. S4d) to maintain the initial pumping rate (Fig. S6a). In year 48, the drawdown constraint is violated so the pumping rate (Fig. S6a) is reduced because the deepening in year 16 extended the well to the total depth of the aquifer and further deepening is not possible. Groundwater pumping ceases after year 51 because the depletion limit of 25% is reached in year 51. Deepening in year 16 increases the total well length (Fig. S4d) and the aquifer saturated thickness intersected by the well (Fig. S4e), which also increases the Transmissivity (Fig. S5b). The increased Transmissivity due to deepening reduces the drawdown (Fig. S6d) as the higher Transmissivity results in less drawdown at the well pumping rate compared to before the deepening. When the well yield is reduced in year 48, the well area served and total number of wells in the grid cell are increased so each well still meets the annual ponded depth target.

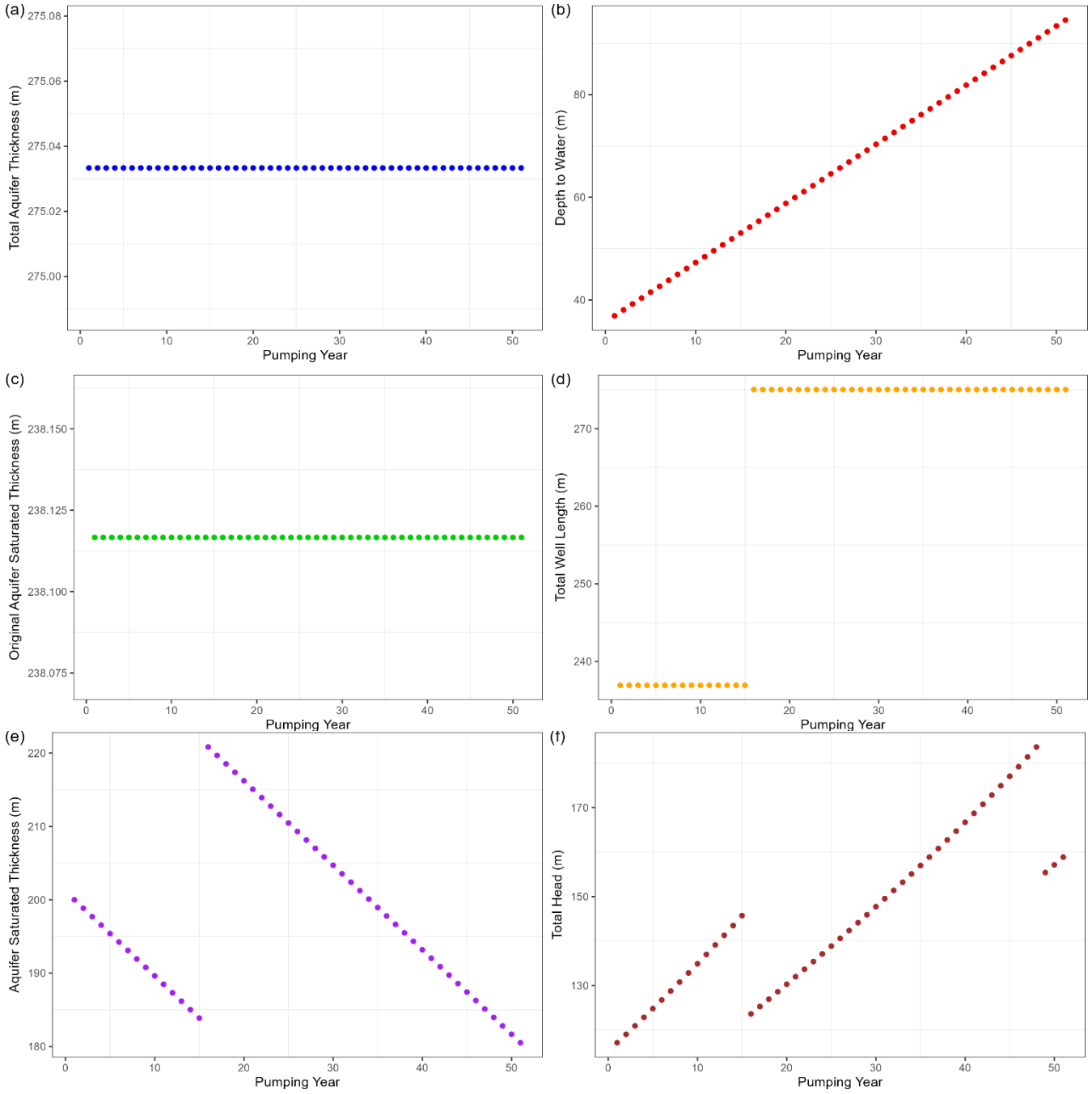

Fig. S4: Aquifer Depths and Thicknesses: (a) Total Aquifer Thickness (m), (b) Depth to Water (m) reflecting changes in groundwater levels due to pumping, (c) Original Aquifer Saturated Thickness (m) showing initial saturated aquifer thickness in first year of pumping, (d) Total Well Length (m) indicating well infrastructure depth, (e) Aquifer Saturated Thickness (m) showing changing thickness in response to changing well depth and (f) Total Head (m) demonstrating the hydrostatic and structural responses of the aquifer system to the changes in well yield and well depth.

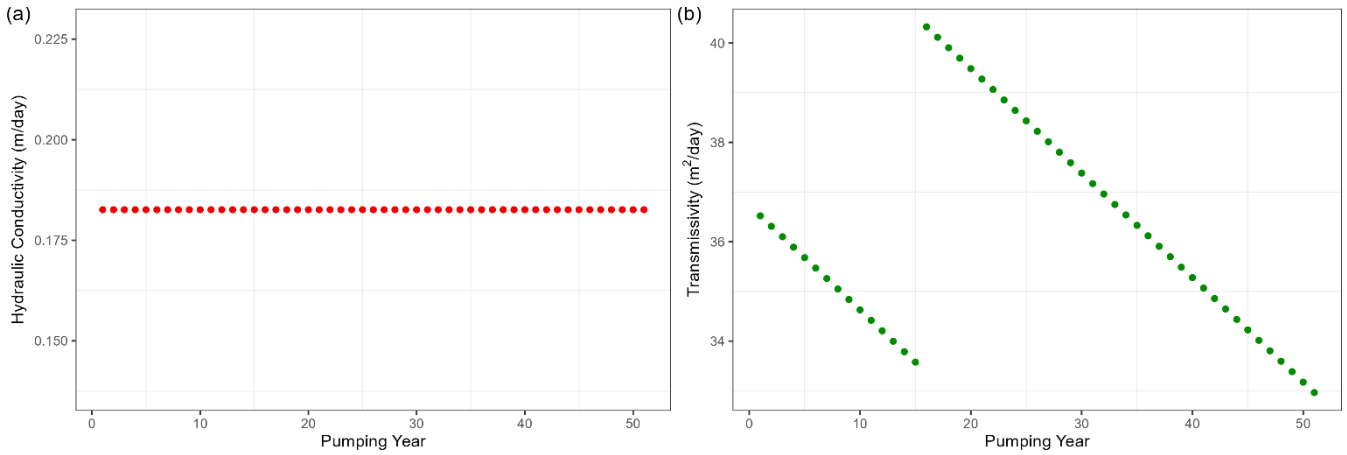

Fig. S5: Aquifer hydraulic properties: (a) Transmissivity ($T = Kb$; m^2/day) and (b) hydraulic conductivity (K; m/day) showing the changing T in response to changing saturated aquifer thickness (b; m)

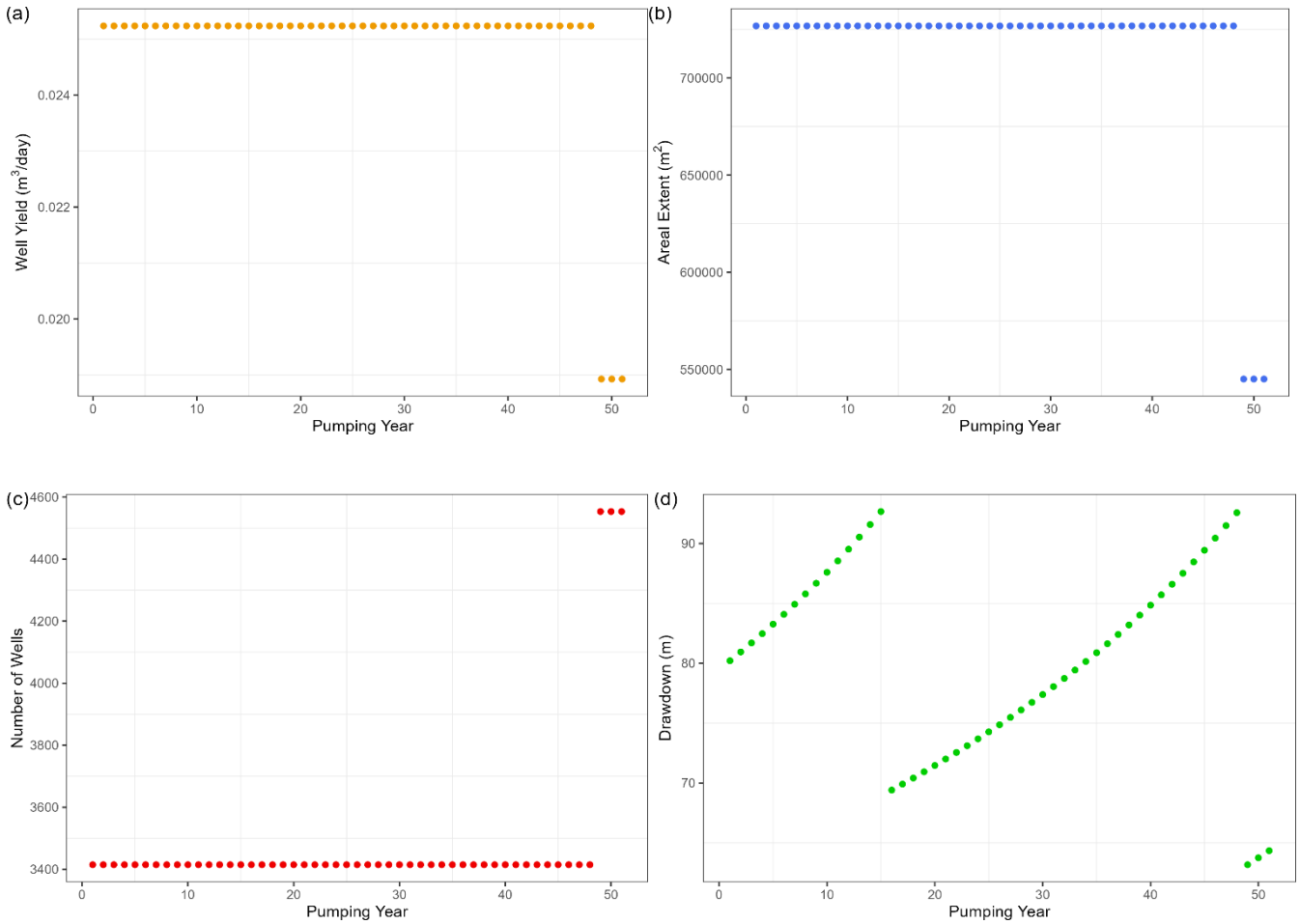

Fig. S6: Well hydraulics: (a) Well Yield (m³/day; *Q*) showing the volume of water extracted per day (specified from a pre-defined array of possible pumping rate. *Q* reduces if the aquifer depth is not able to support pumping volumes), (b) Areal Extent (m²) indicating the spatial coverage of pumping from a well in a grid cell, (c) Number of Wells in a grid cell, and (d) Drawdown (m) illustrating the impact of pumping on groundwater levels near the well head.

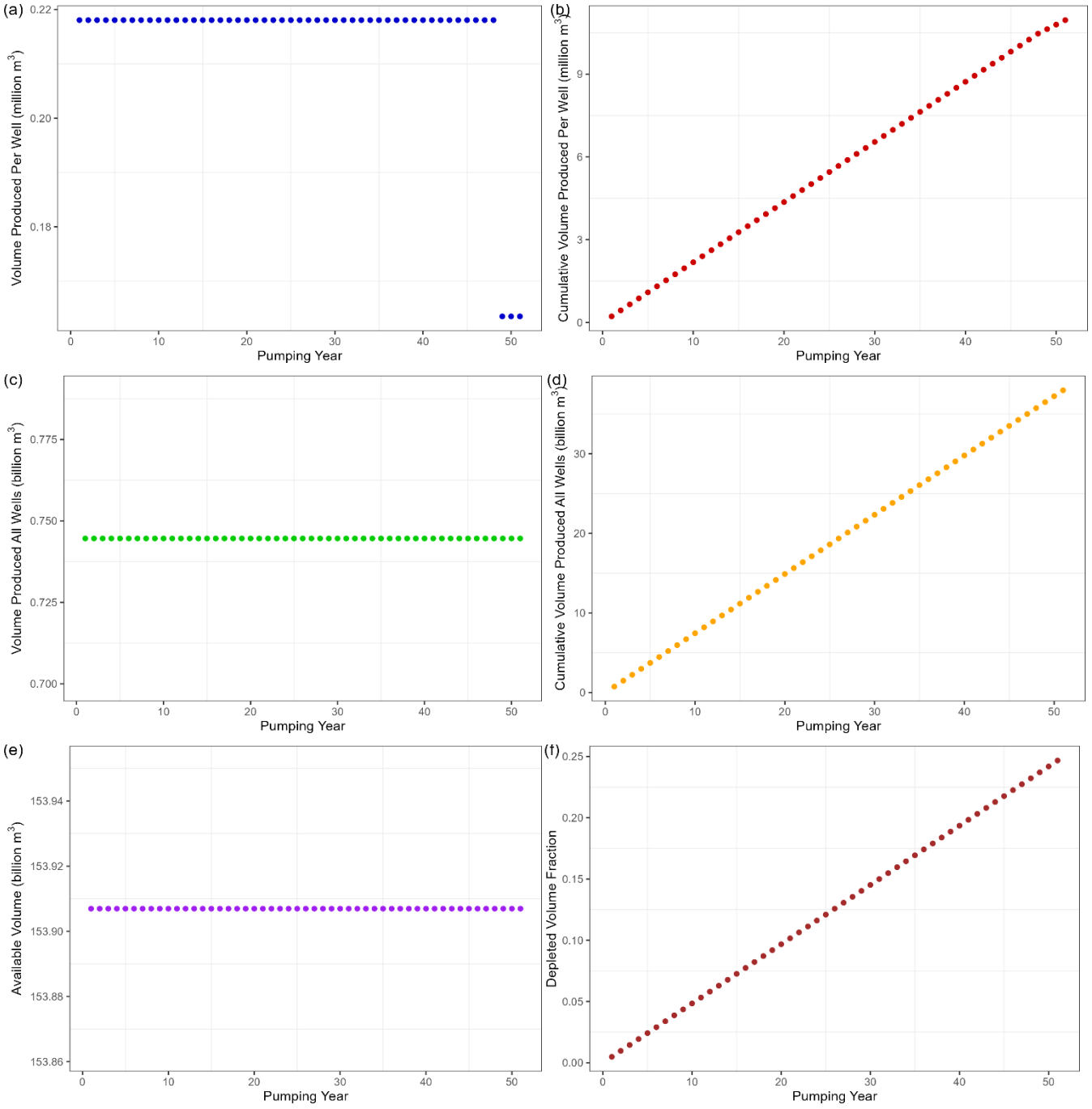

Fig. S7: Groundwater volumes (extraction and availability): (a) Volume produced per well (million m³) and (b) Cumulative volume produced per well (million m³) showing individual well productivity over time in this grid cell, (c) Total volume produced by all wells (billion m³) and (d) Cumulative volume produced by all wells (billion m³) showing the total groundwater extraction, with (e) Available volume (billion m³) calculated using aquifer properties, and (f) Depleted Volume Fraction indicating the ratio between resource availability and depletion over time (until the depletion limits are met, in this case 25%).

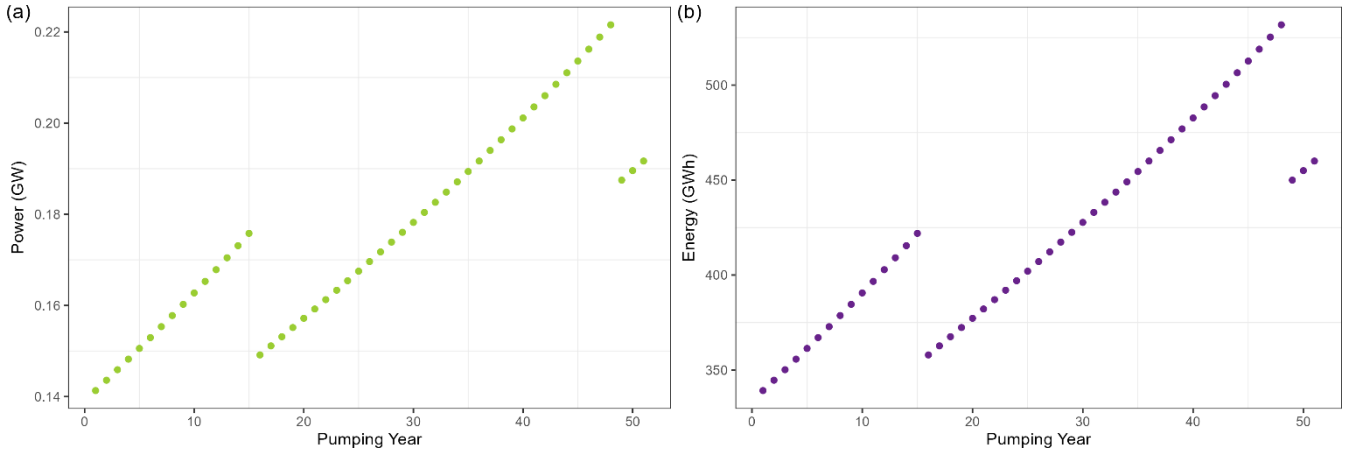

Fig. S8: Energy and power to pump groundwater: (a) Power (GW) and (b) Energy (GWh) showing the energy requirements associated with groundwater extraction.

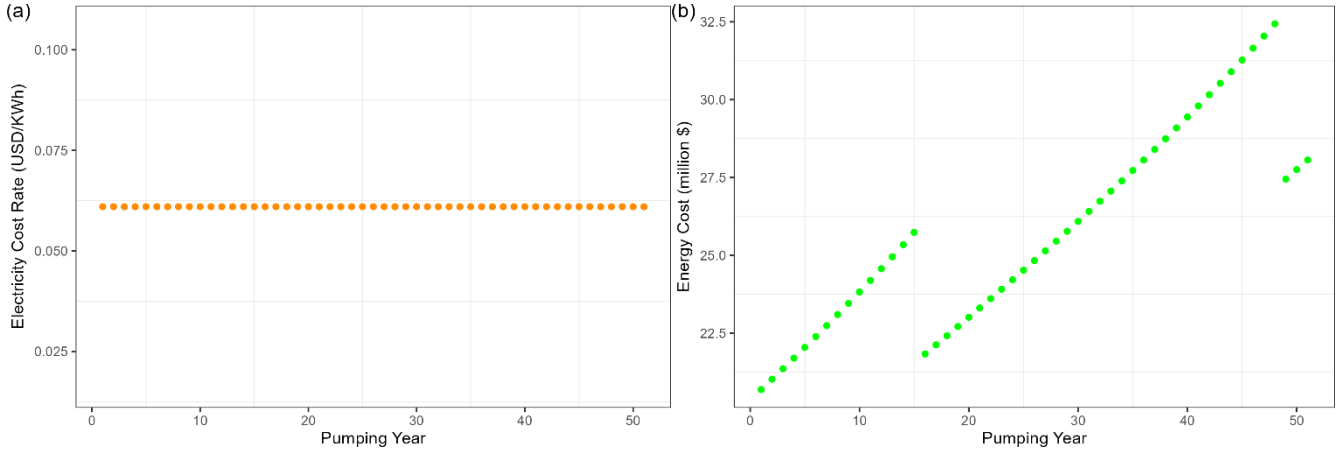

Fig. S9: Energy costs: (a) Energy Cost Rate (USD/KWh) representing electricity cost rate in this grid cell and (b) Energy Cost (million $)

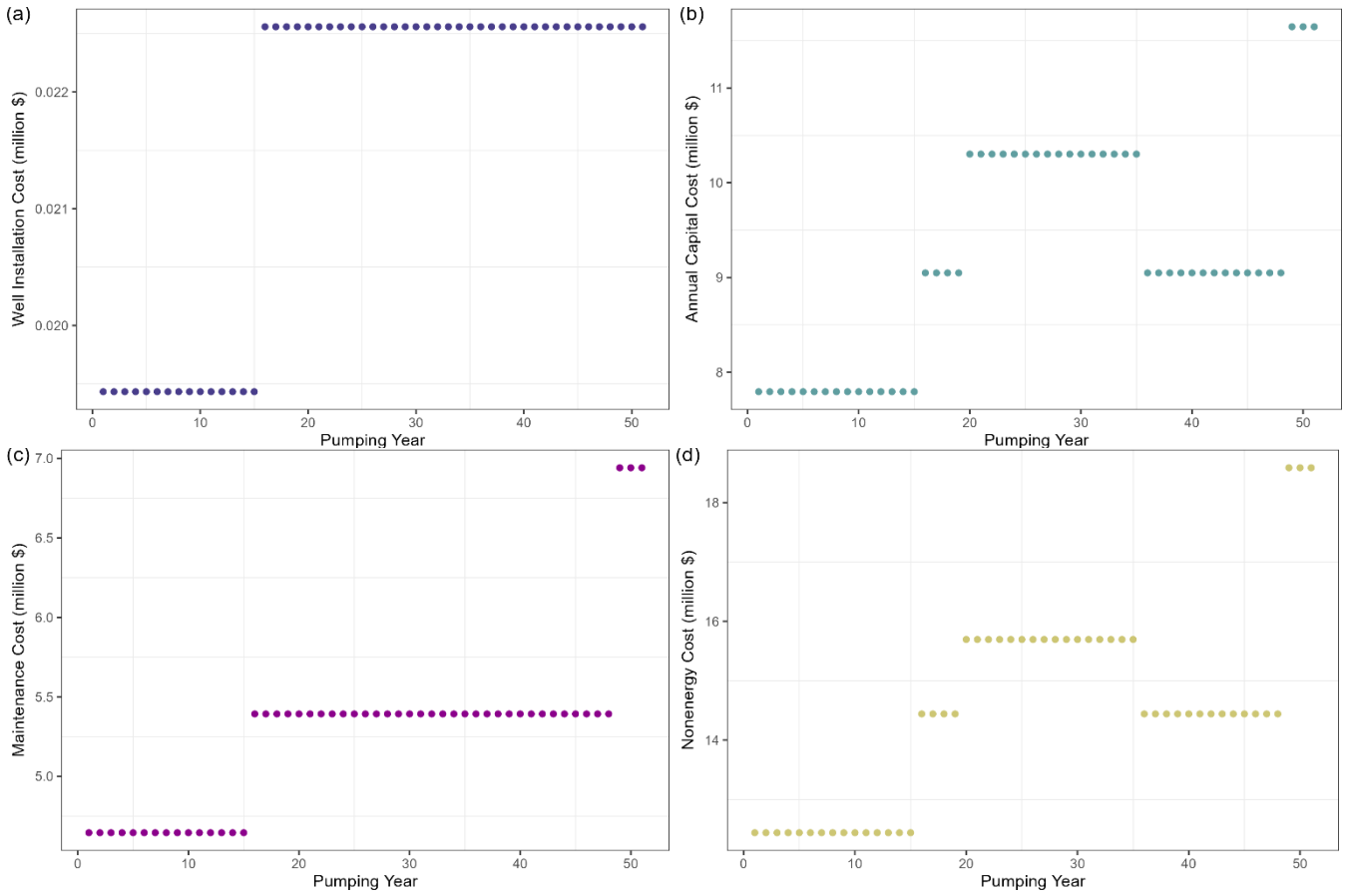

Fig. S10: Nonenergy cost and its components: (a) Well Installation Cost (million $), (b) Annual Capital Cost (million $), (c) Maintenance Cost (million $), and (d) Nonenergy Cost (million $) covering various non-energy cost components associated with infrastructure requirements of pumping groundwater.

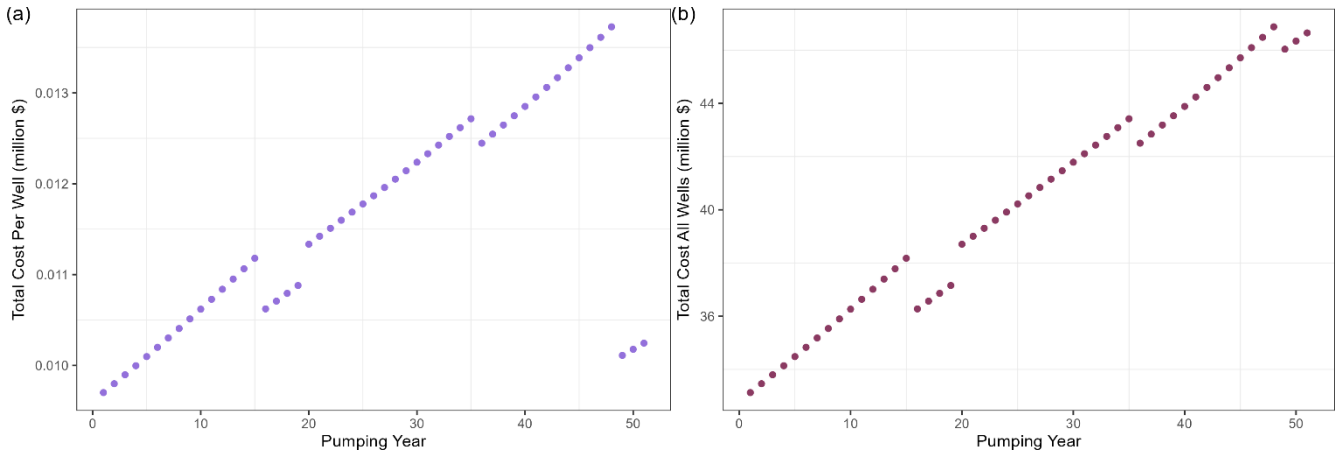

Fig. S11: Total costs of groundwater extraction: (a) Total Cost Per Well (million $) and (b) Total Cost All Wells (million $) in this grid cell showing the overall cost burden of groundwater extraction for this grid cell in a moderate extraction scenario

95

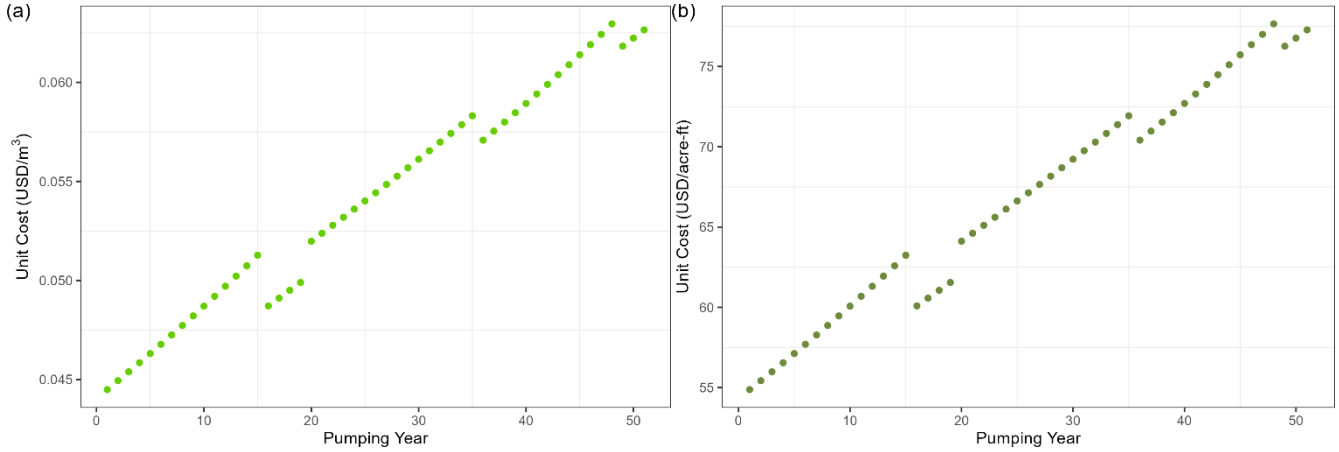

Fig. S12: Unit costs of groundwater supply: (a) Unit Cost (USD/m³) and (b) Unit Cost (USD/acre-ft) providing insight into the cost-effectiveness and productivity of this grid cell (*unit cost = total volume produced / total cost of production*).

100

S3 Processing and Results Maps

This section provides spatial details on a 0.5-degree gridded resolution using global maps of key inputs (Niazi et al., 2024b) and outputs (Niazi et al., 2024a) of superwell in a moderate depletion (25%) and low ponded depth target scenario (0.3m) (Niazi et al., 2025).

S3.1 Hydraulics

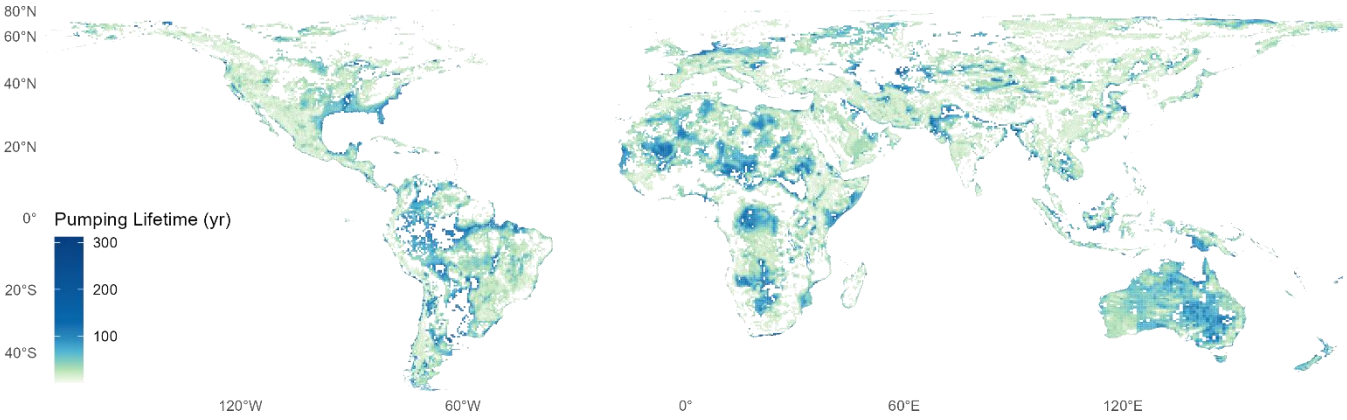

Fig. S13: Pumping lifetime (year)

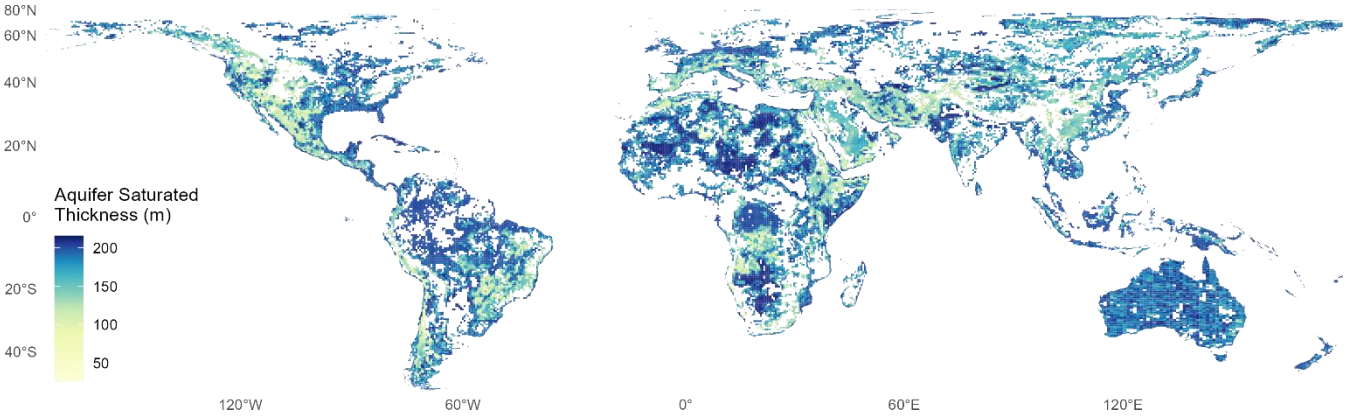

Fig. S14: Aquifer saturated thickness (m)

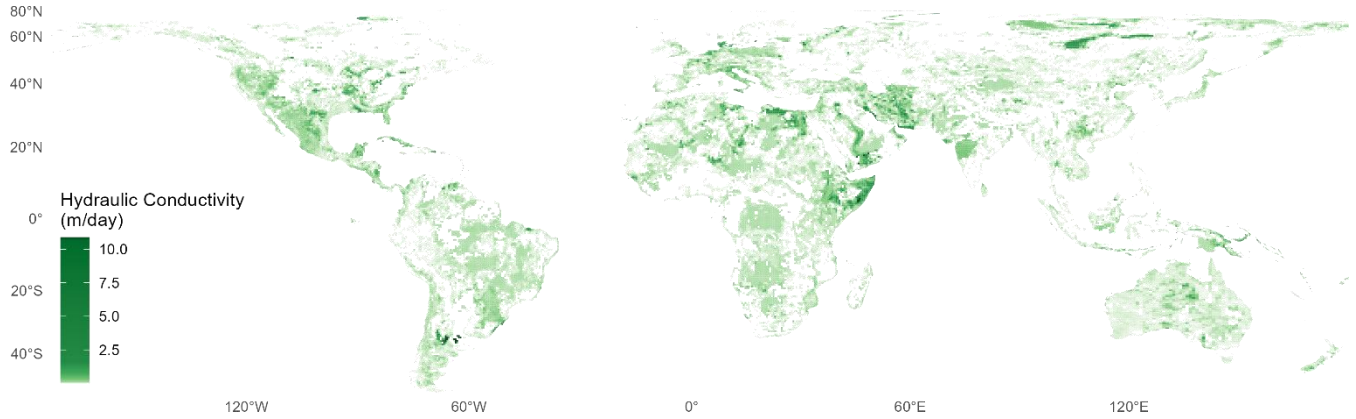

Fig. S15: Hydraulic conductivity (m/day)

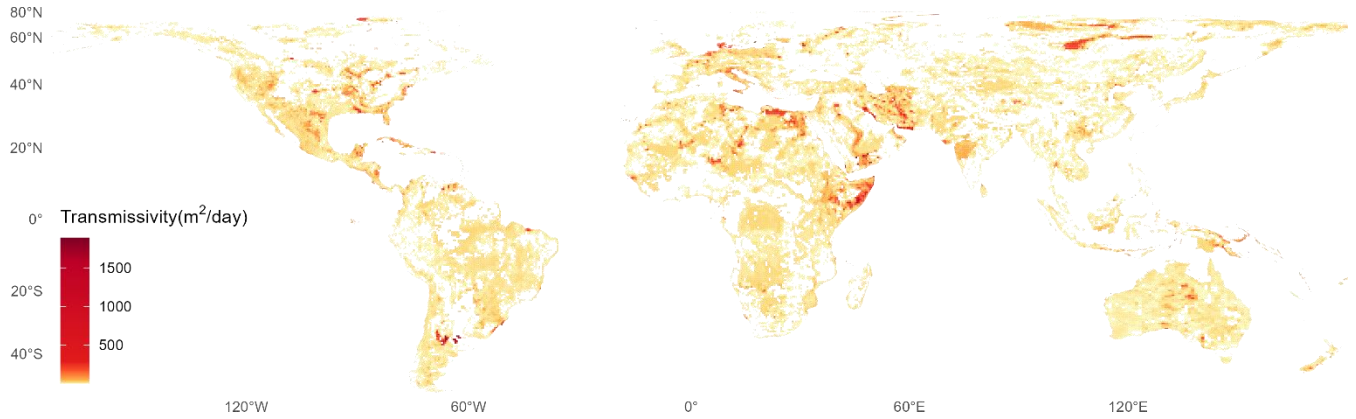

Fig. S16: Transmissivity (m^2/day) averaged over all pumping years

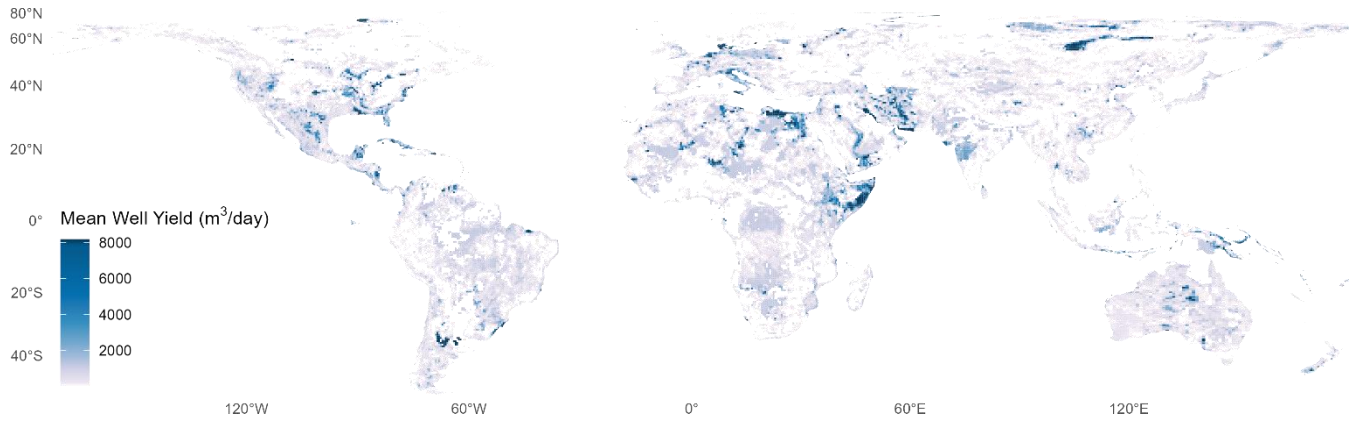

Fig. S17: Well yield (m^3/day) averaged over pumping lifetime

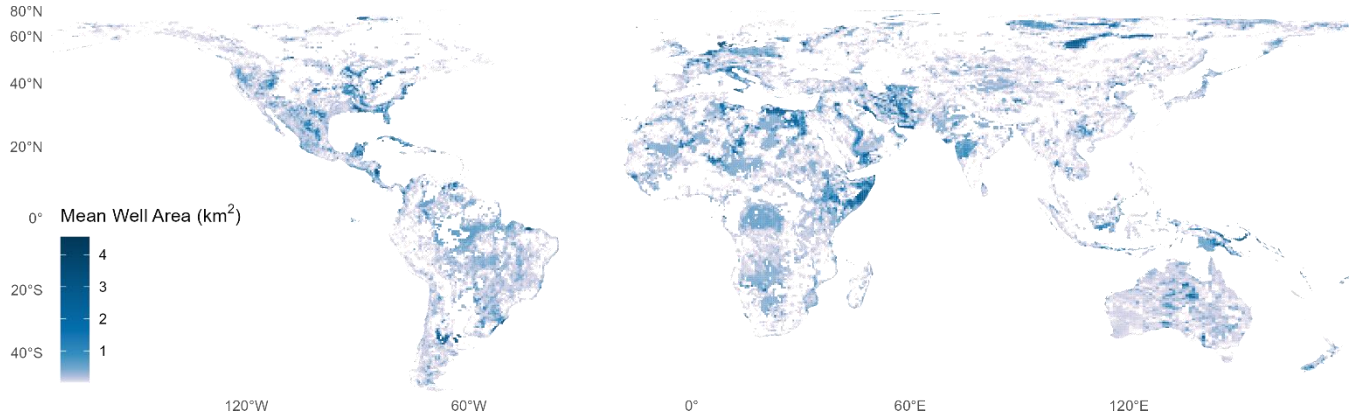

Fig. S18: Well area (km^2) averaged over pumping lifetime

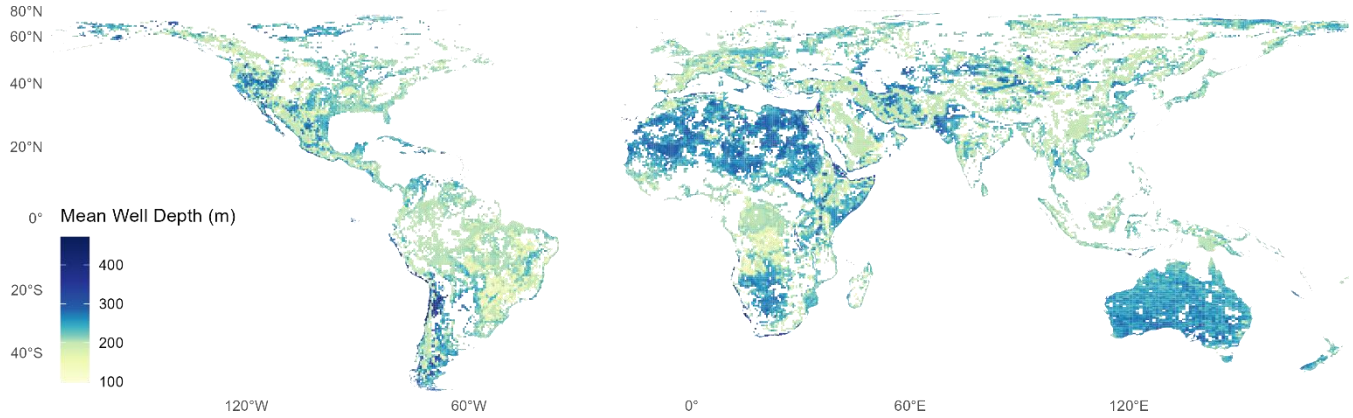

125

Fig. S19: Total well length (well depth; m) averaged over pumping lifetime

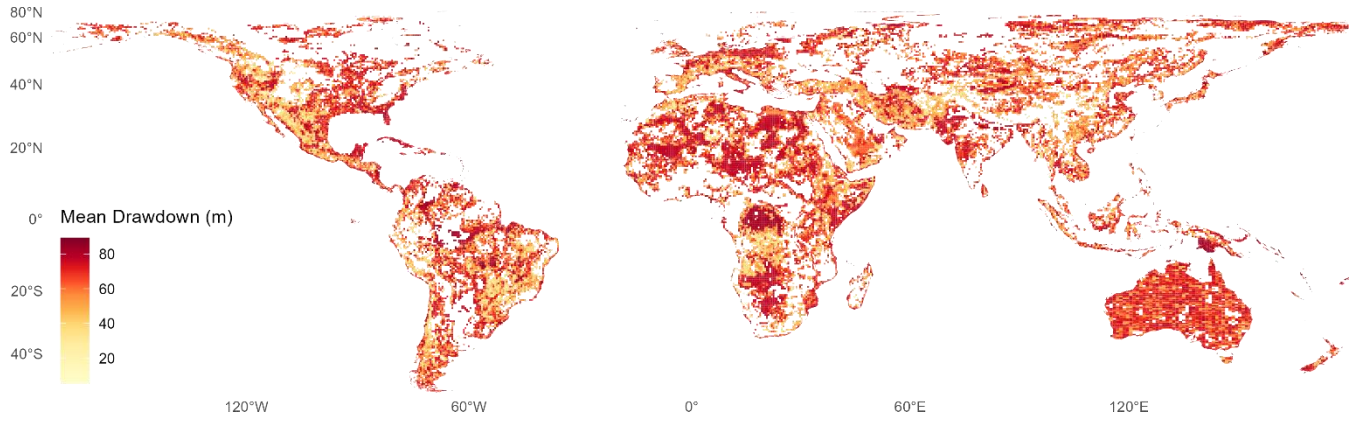

Fig. S20: Drawdown (m) averaged over pumping lifetime

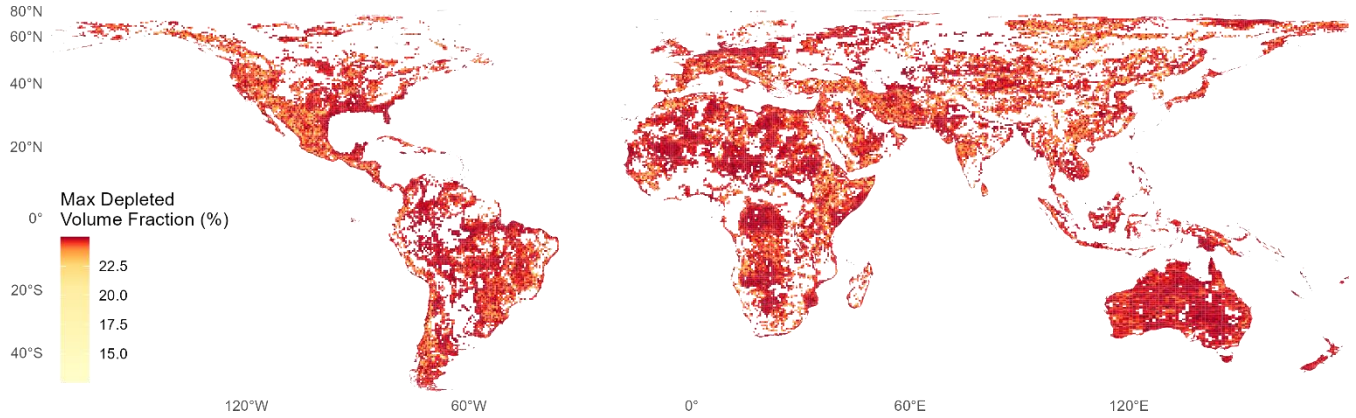

Fig. S21: Maximum fraction of depleted volume i.e., volume produced over available volume, also referred to as depletion limit

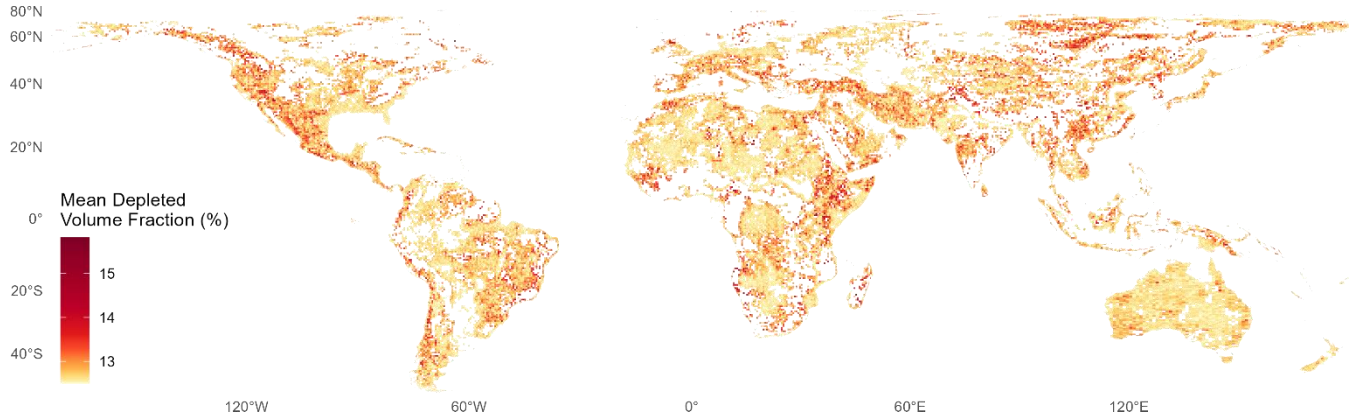

Fig. S22: Mean fraction of depleted volume i.e., volume produced over available volume, averaged over pumping lifetime

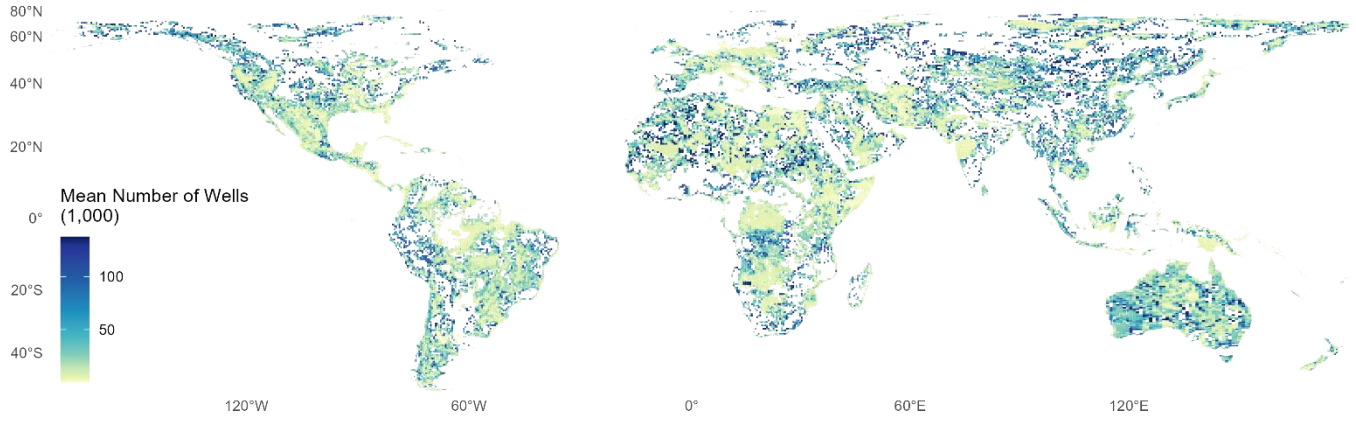

Fig. S23: Number of well in a grid cells (x1000)

S3.2 Costs

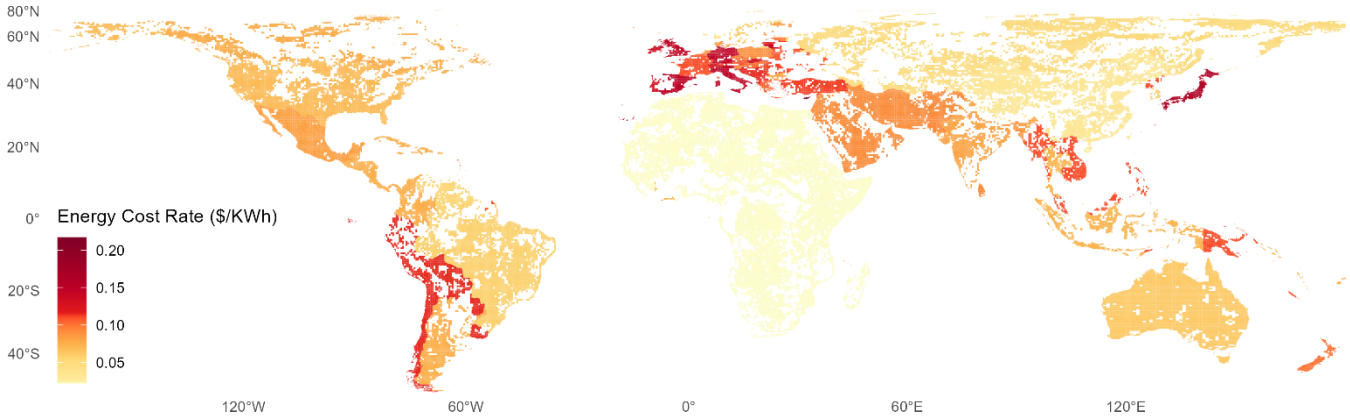

Fig. S24: Electricity cost rate (2016 USD/KWh) for 172 countries downscaled to all grid cells. 0.074 (USD/KWh) is assumed to fill missing grid cells.

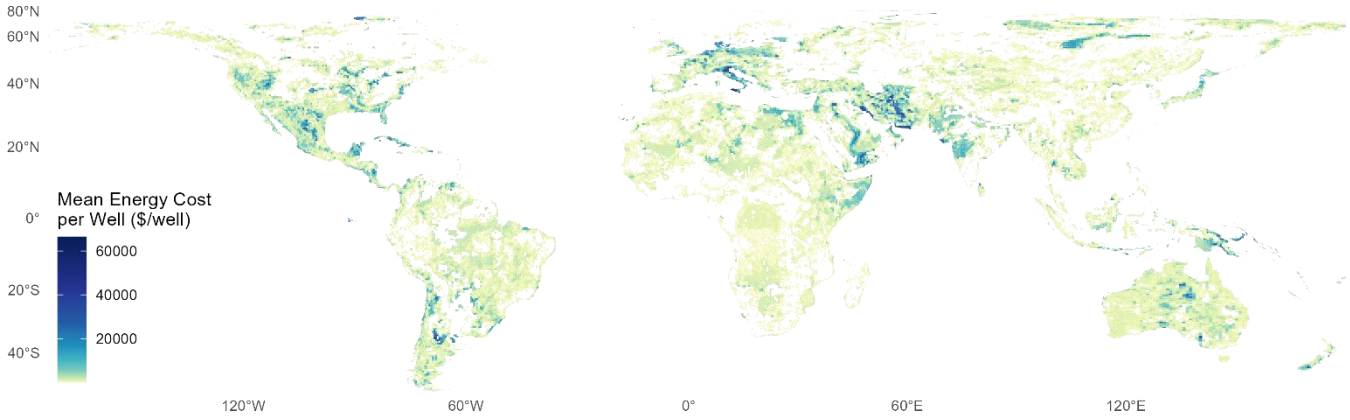

Fig. S25: Energy cost per well (USD/well)

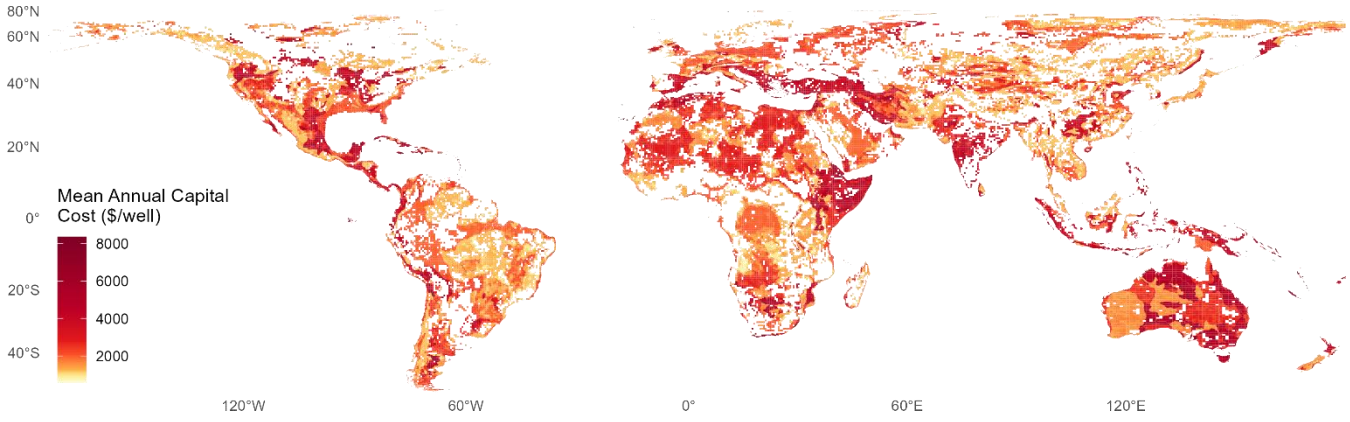

Fig. S26: Annual capital cost per well (USD/well) averaged over pumping lifetime

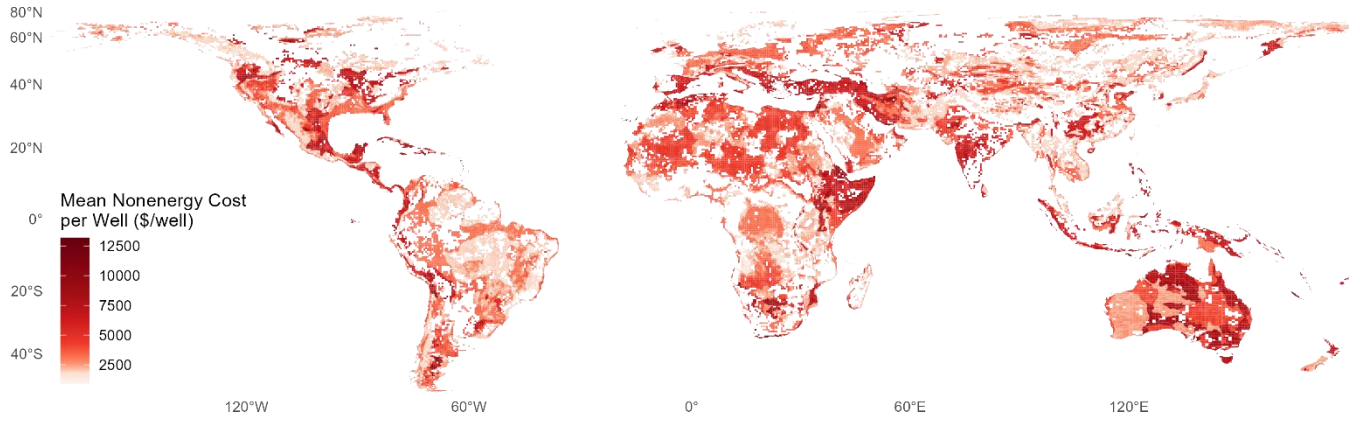

Fig. S27: Non-energy cost per well (USD/well) averaged over pumping lifetime

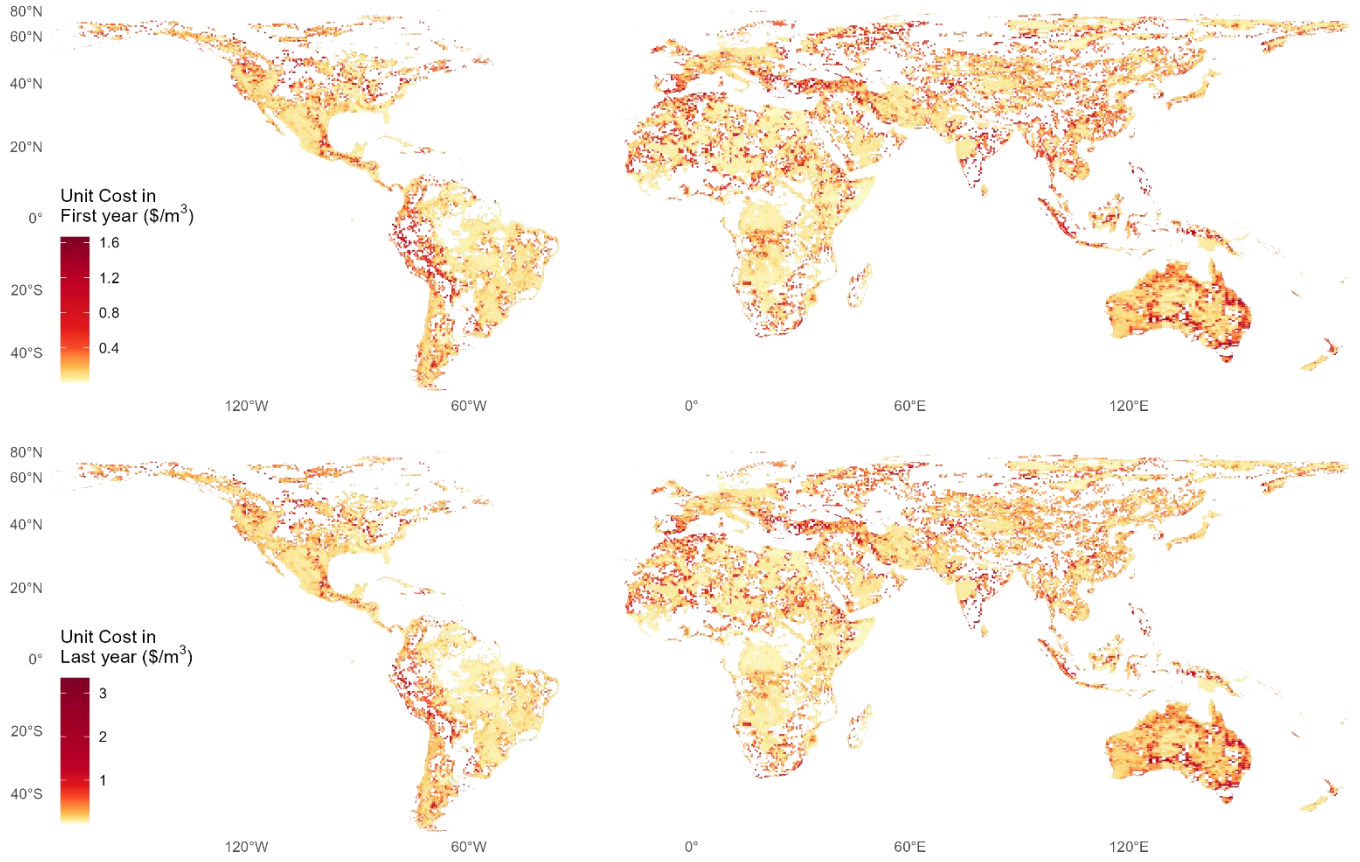

Fig. S28: Unit cost (USD/m^3) in first and last year of pumping

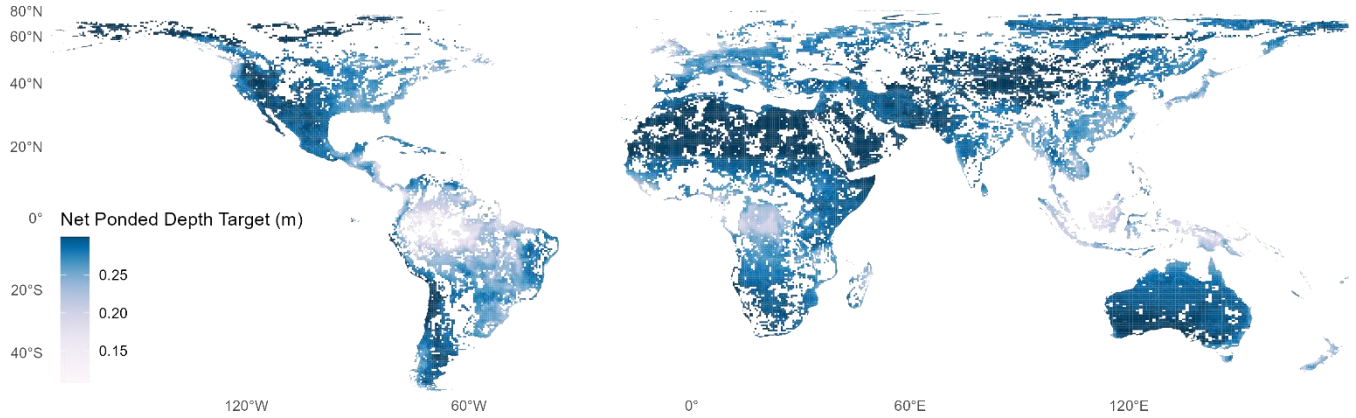

Fig. S29: Recharge-adjusted net ponded depth target for the moderate depletion scenario (0.3m ponded depth, 25% depletion limit)

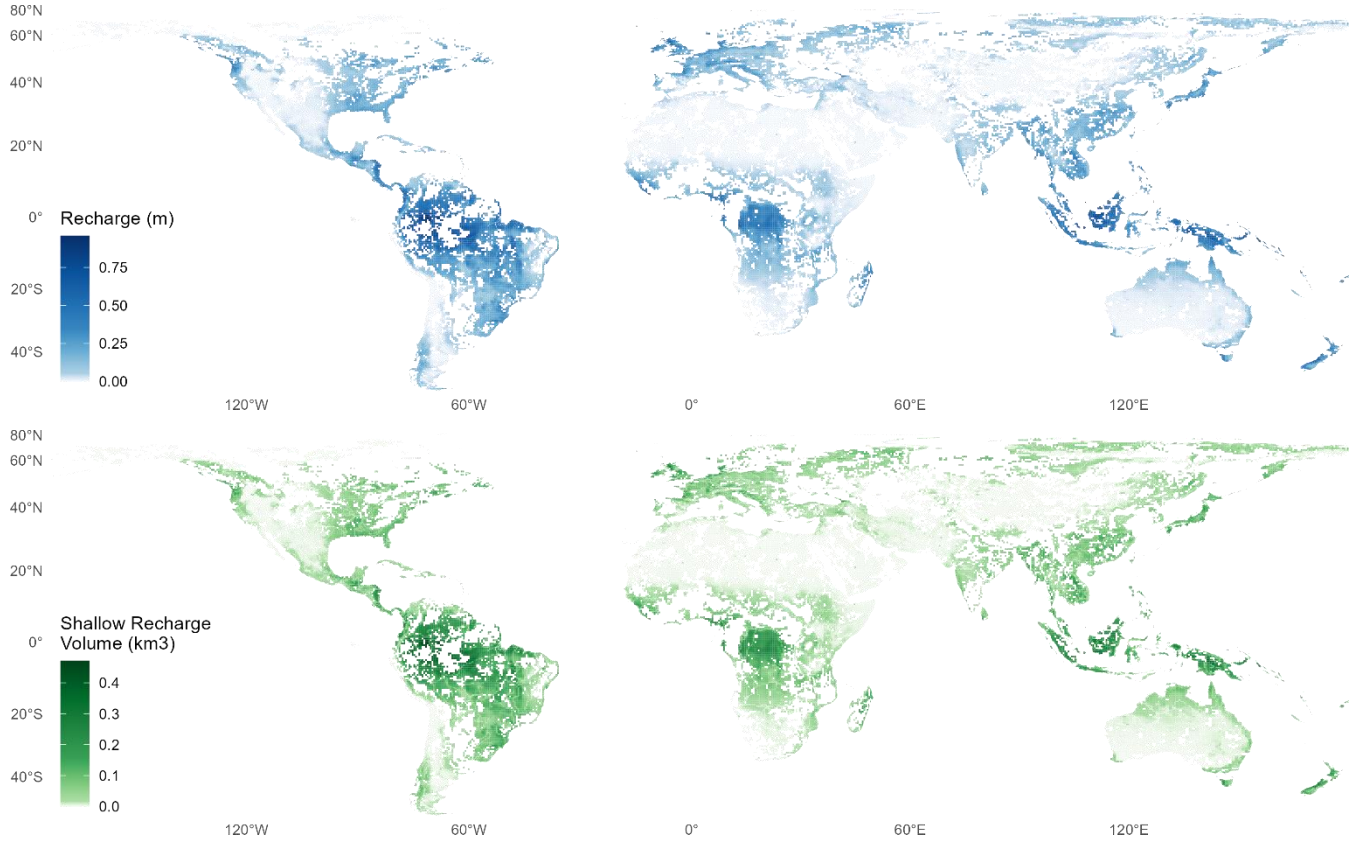

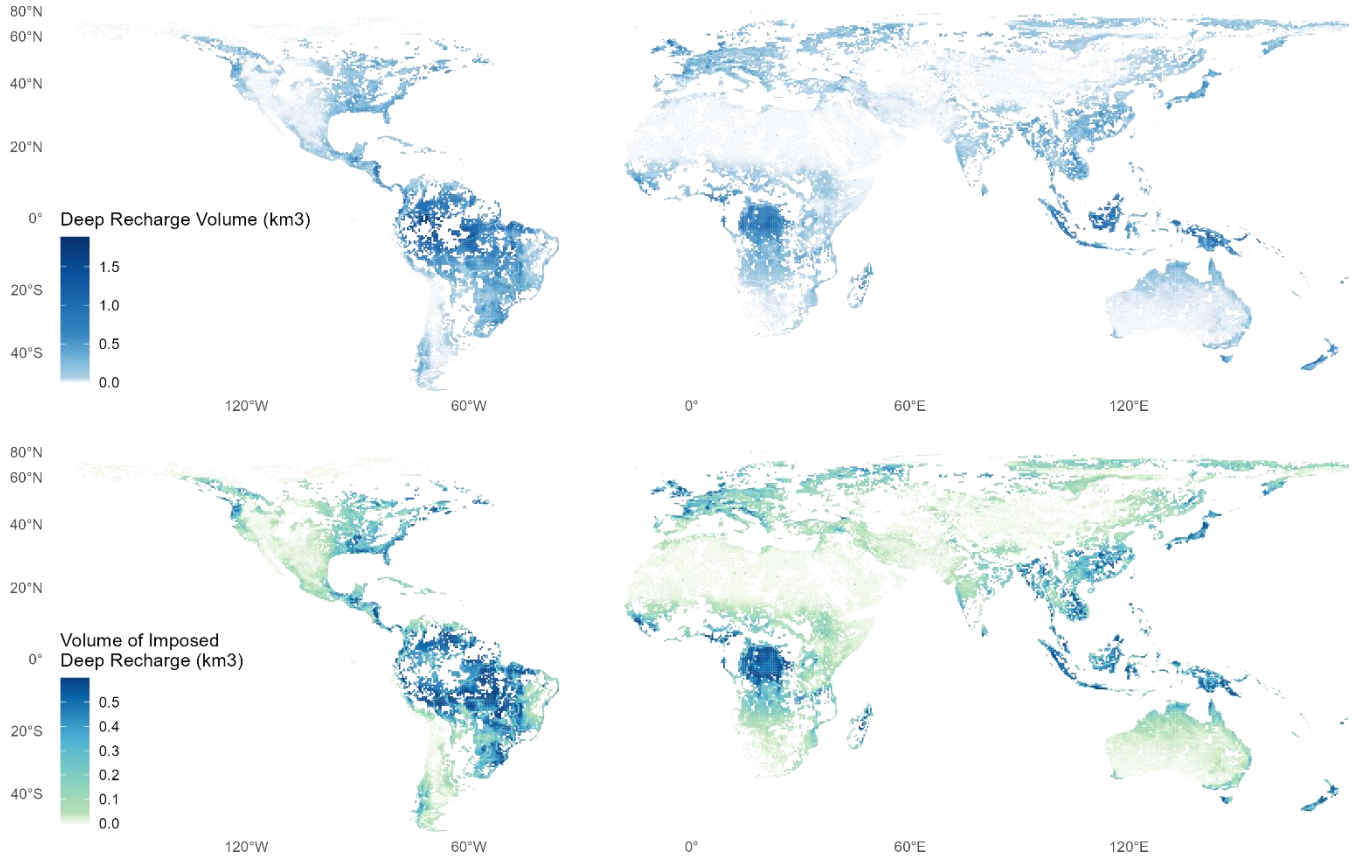

160 **Fig. S30: Recharge rates (m/year), shallow and deep partioned recharge volumes (km3), and imposed deep recharged volume (minimum of volume pumped and deep recharge volumes) to avoid accumulation and depth to water reductions**

165

S4 Timeseries of Key Global Variables

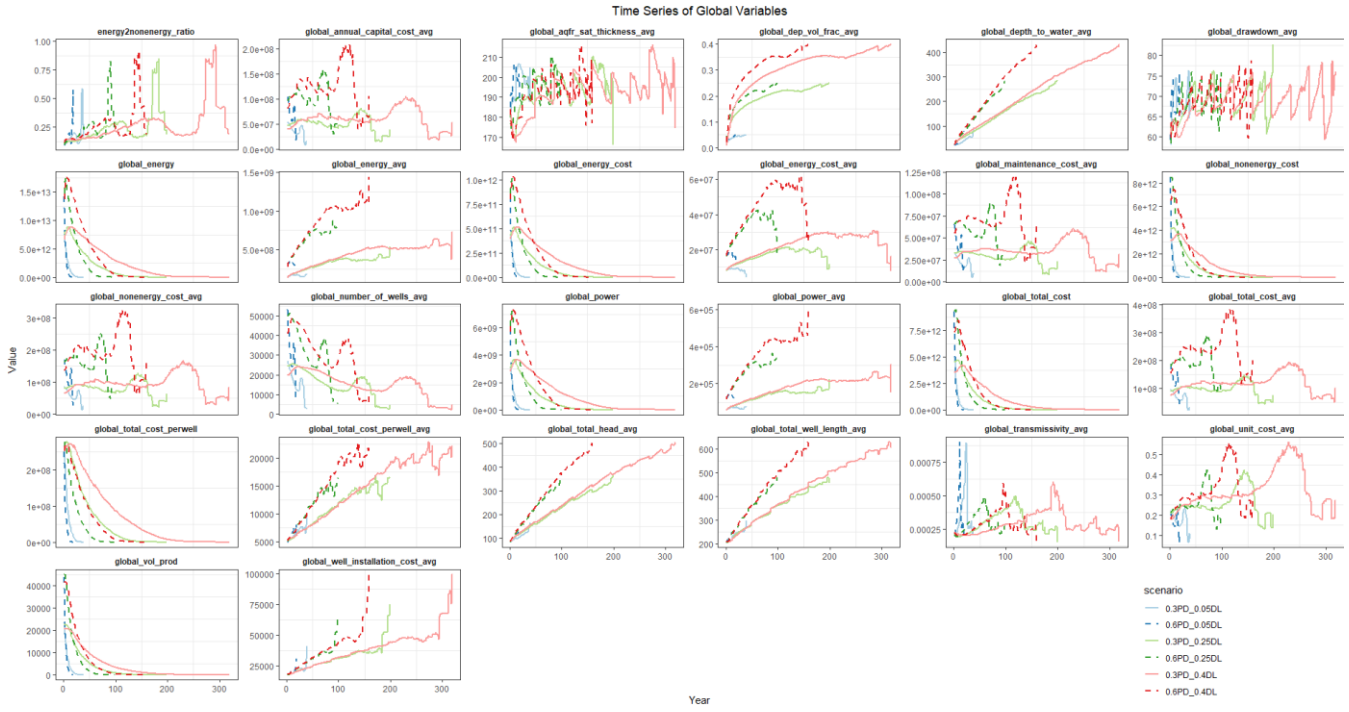

Fig. S31: Timeseries of all key global variables produced by superwell across six scenarios (DL = Depletion limit, PD = Ponded depth). Note some plots have log scale on x-axis. Global average implies a mean across all grid points in a given year of pumping simulation.

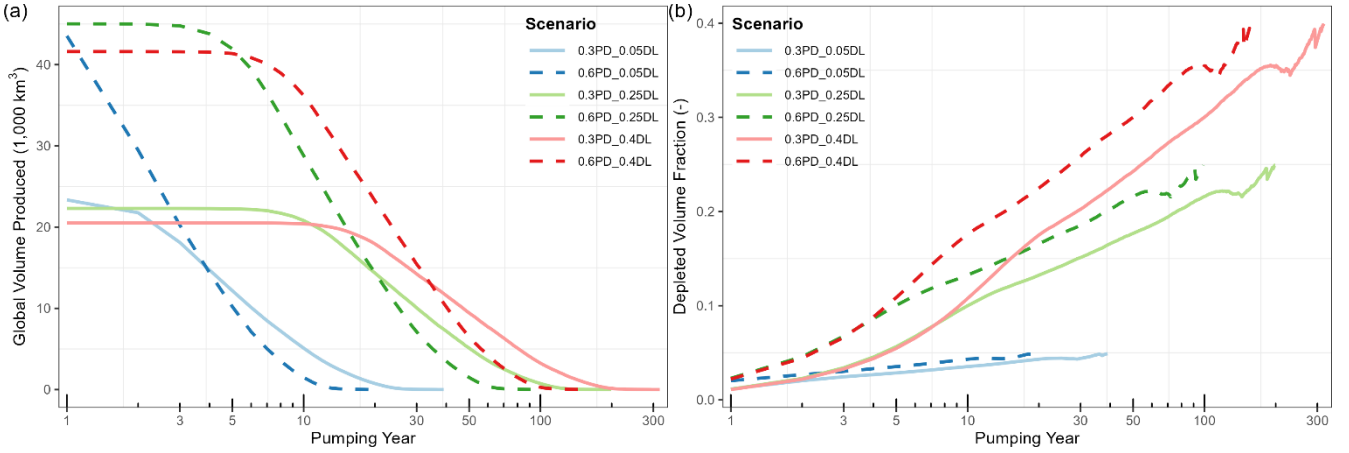

Fig. S32: Global pumping volume characteristics: (a) Global volume pumped (1000 km^3) and (b) depletion volumes fraction representing volume pumped over available volume globally in a year of pumping. Note the log-scale on x-axis

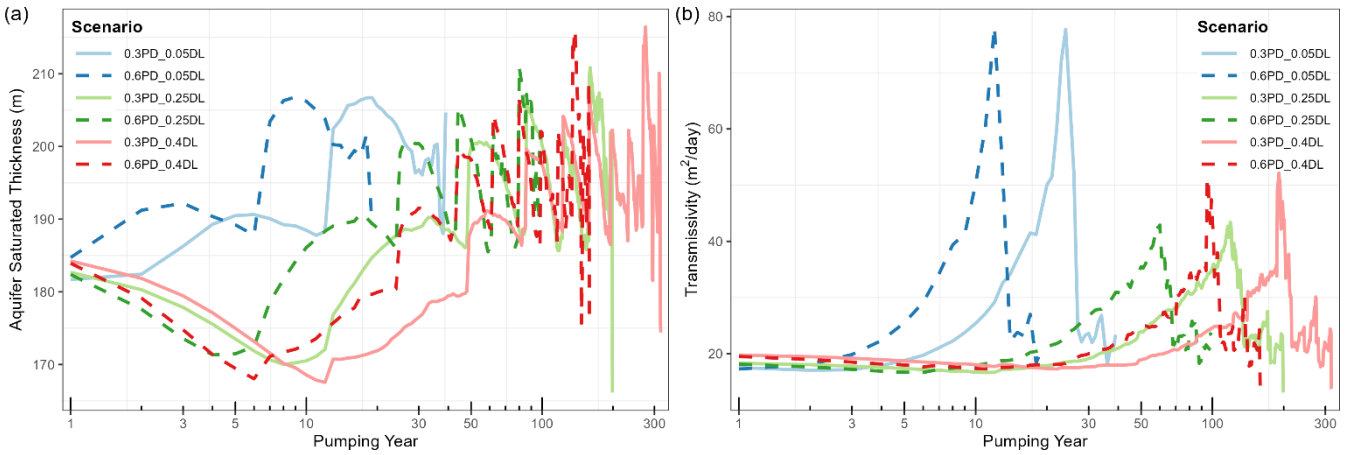

Fig. S33: Aquifer characterises: (a) saturated aquifer thickness (m) and (b) transmissivity (m^2/day) that get updated as wells are deepened over time. Note the log-scale on x-axis

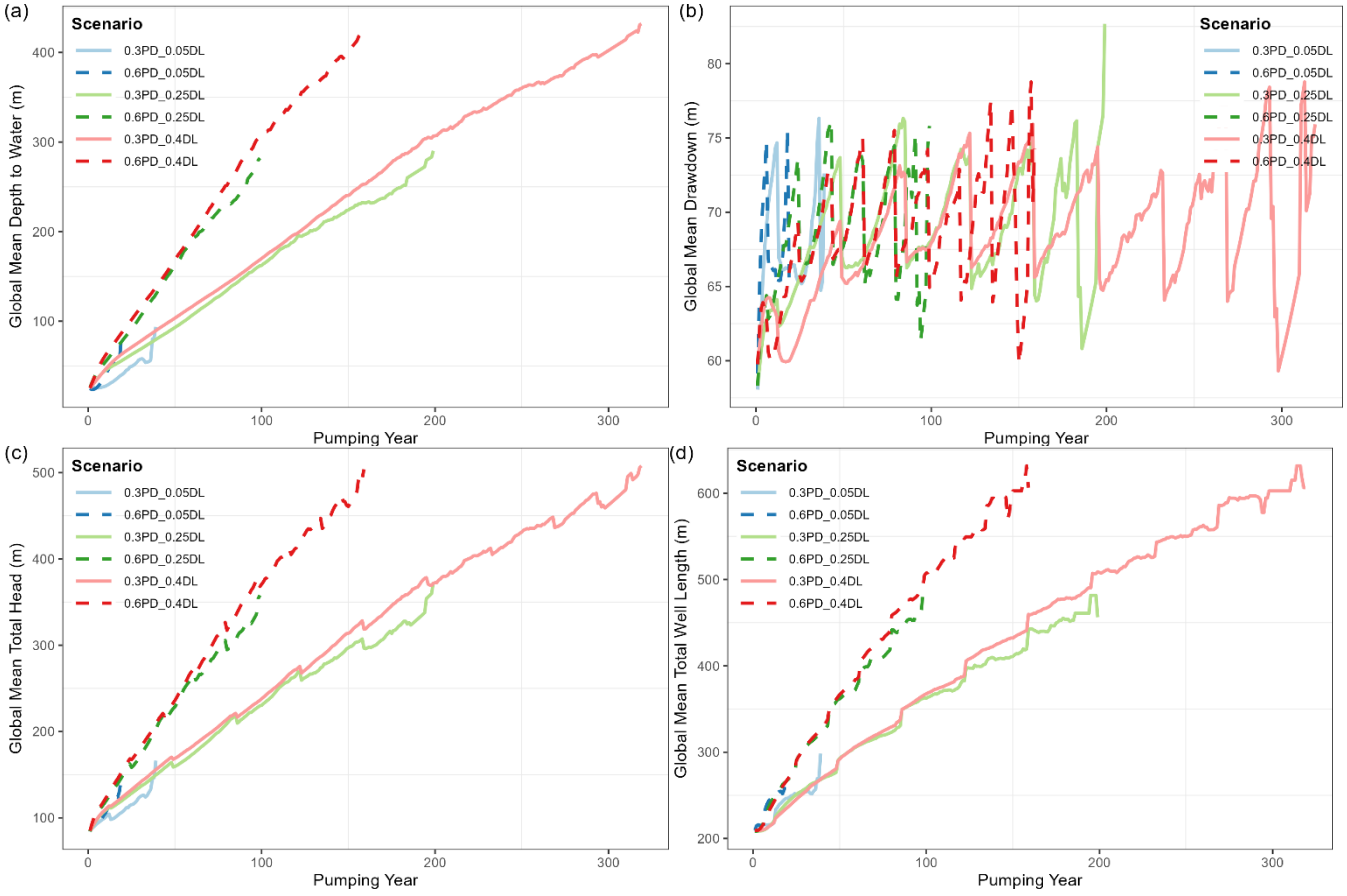

Fig. S34: Depth characteristics averaged across all grid cells in a model pumping year: (a) Global mean depth to water (m), indicating the average depth from the surface to the groundwater level. (b) Global mean drawdown (m), representing the average

decline in groundwater level due to pumping. (c) Global mean total head (m), the average hydraulic head or energy per unit weight of water. (d) Global mean total well length (m), indicating the average length of all wells across all grid cells.

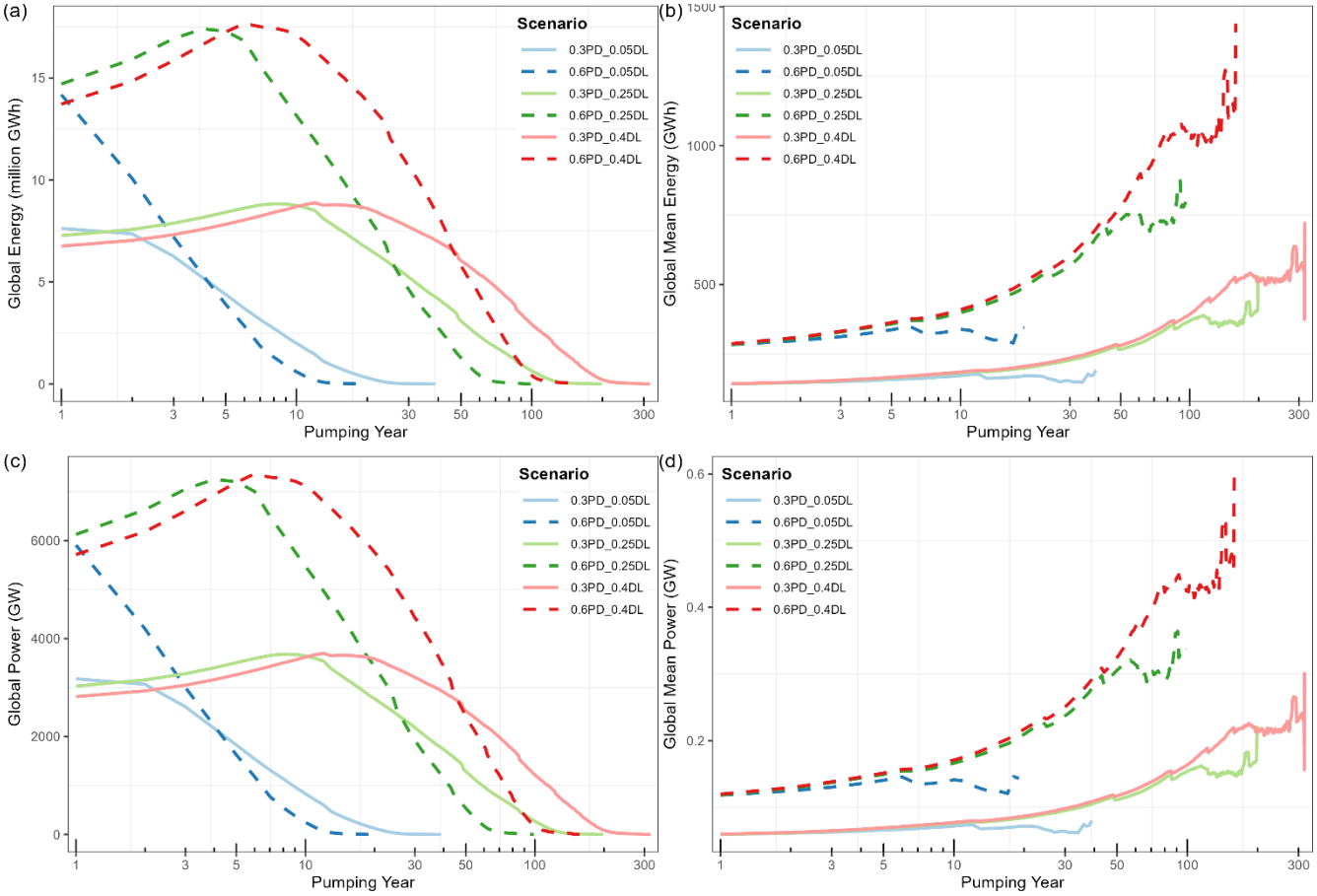

Fig. S35: Energy and power requirements for pumping groundwater in all grid cells in a model pumping year: (a) Total energy used globally to pump groundwater (million GWh); (b) Global mean energy (GWh) representing the average energy used across all grid cells; (c) Total power required to pump groundwater globally; and (d) Global mean power (GW) indicating the average power used across all grid cells. Note the log-scale on x-axis

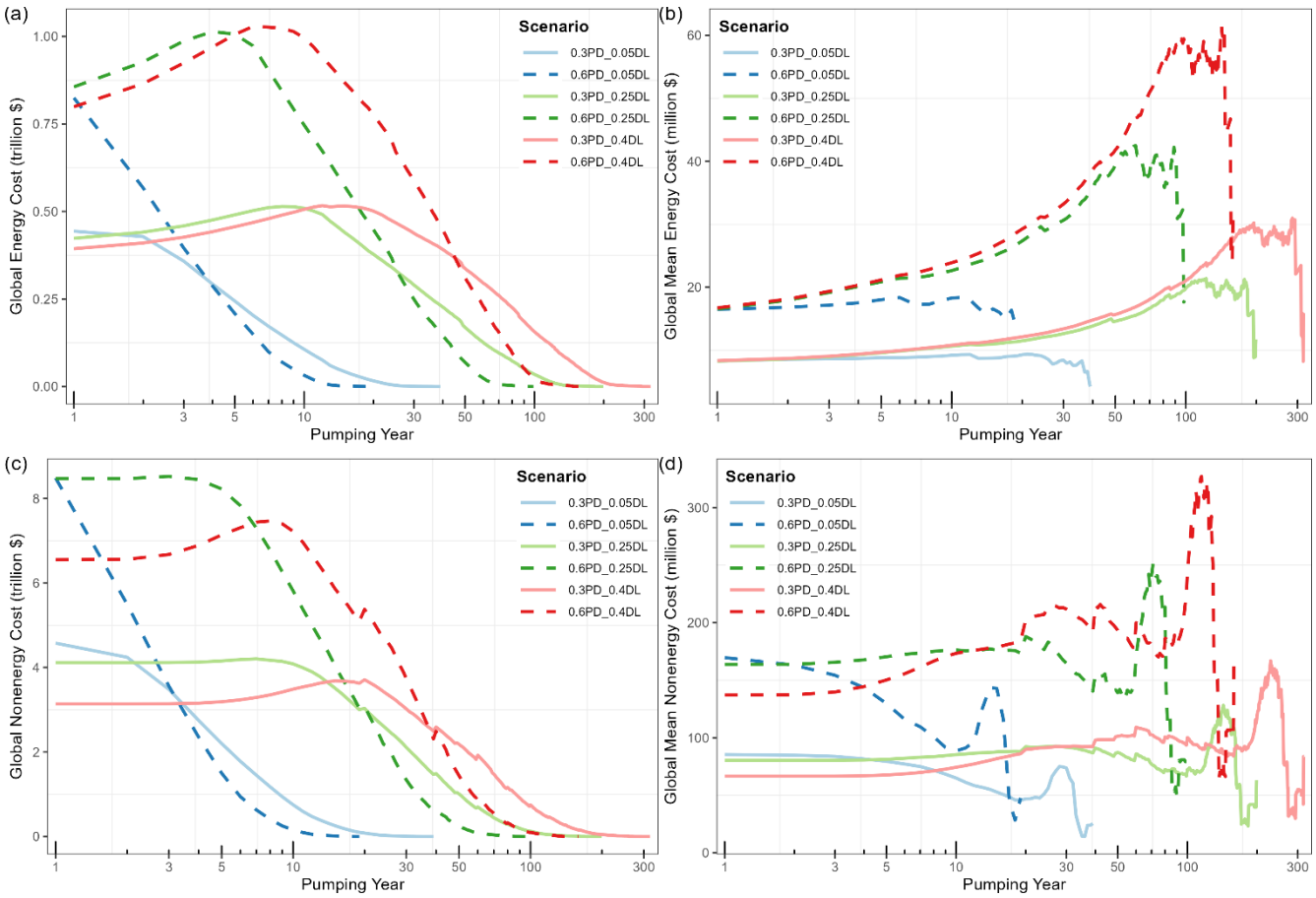

200 **Fig. S36: Global energy and nonenergy costs in all grid cells: (a) Total energy cost globally (trillion USD); (b) Global mean energy cost, representing the average cost of energy (million USD) across all grid cells; (c) Total nonenergy cost globally (trillion USD), representing the total of all costs associated with groundwater extraction excluding energy costs of pumping; (d) Global mean nonenergy cost (million USD), indicating the average nonenergy cost across all grid cells. Note the log-scale on x-axis**

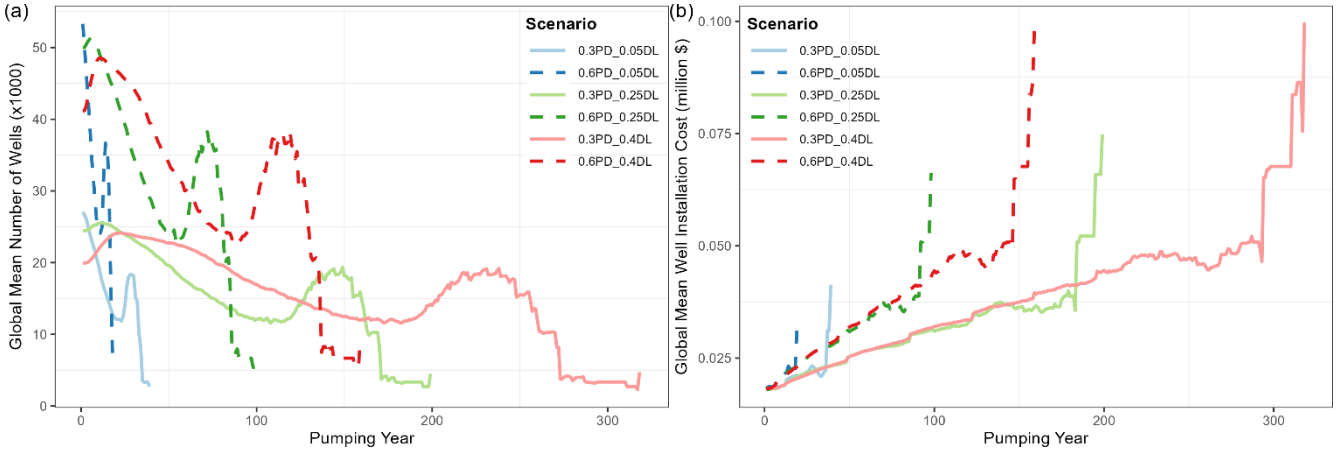

205

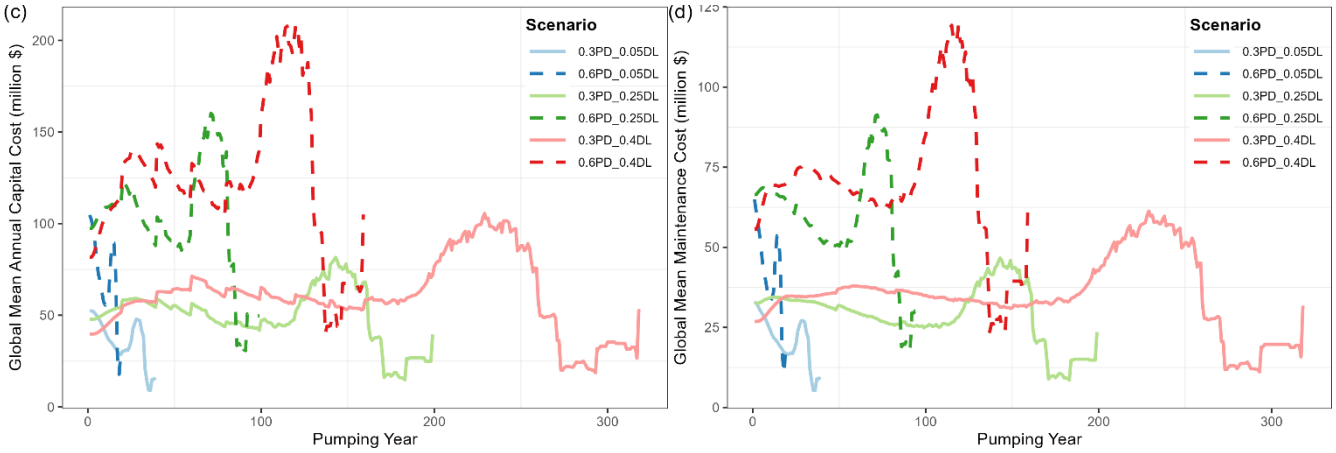

Fig. S37: Nonenergy costs components across averaged across all grid cells in a pumping year: (a) Global mean number of wells required to meet pumping targets (1000s); (b) Global average cost of installing a groundwater well (million USD); (c) Global mean annual capital cost (million USD), representing the average annual cost of capital investments in groundwater infrastructure; (d) Global average cost of maintaining groundwater wells (million USD).

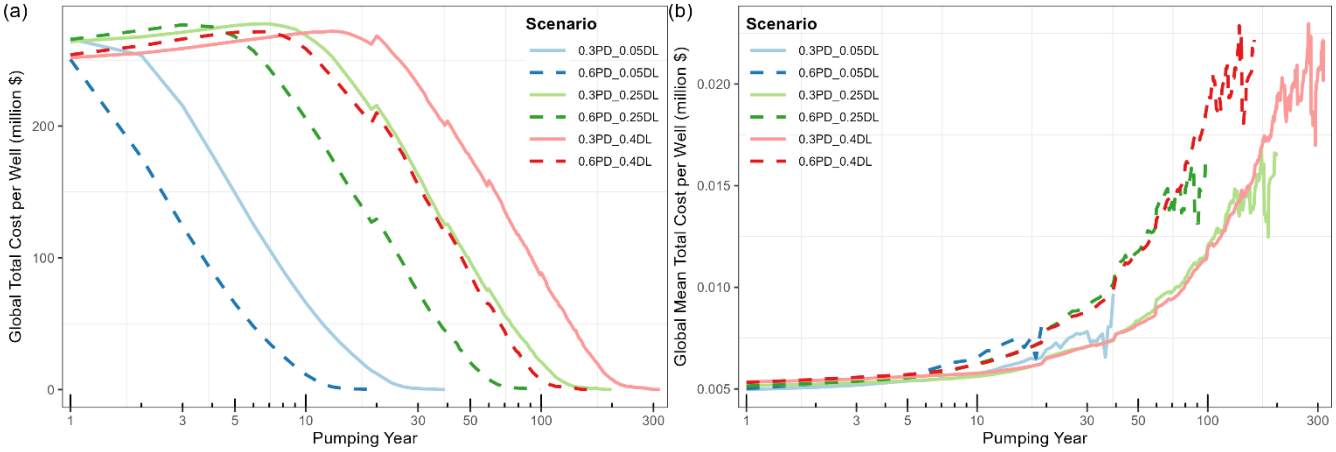

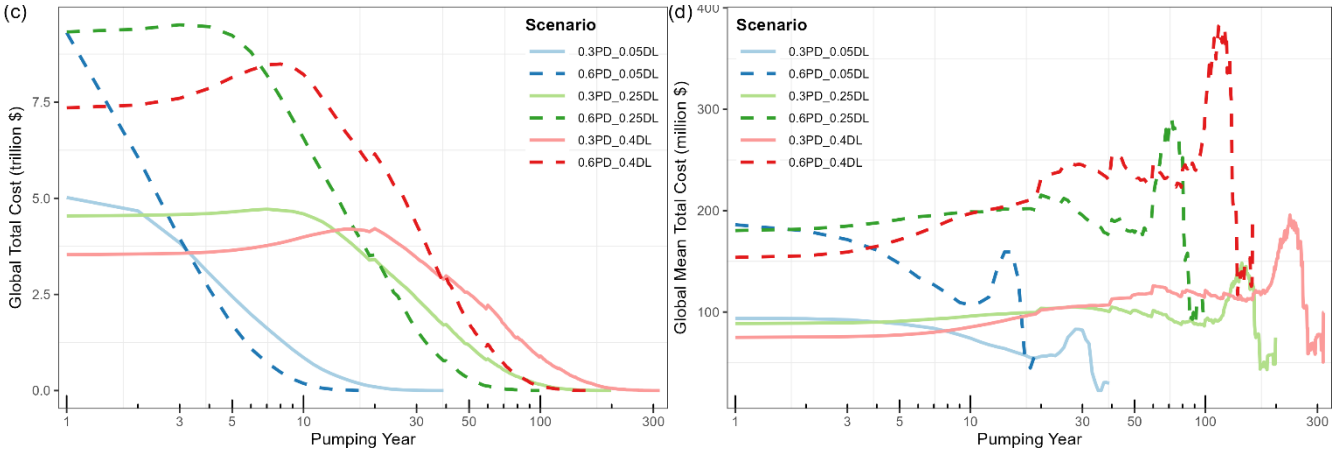

215 **Fig. S38: Global total and mean costs for groundwater extraction globally: (a) Sum of total cost globally per each well (million USD); (b) Global mean total cost per well (million USD), reflecting the average expenditure incurred for each well across all grid cells in a model pumping year; (c) Total cost of groundwater extraction globally (trillion USD); and (d) Global mean total cost (million USD), denoting the average cost of groundwater extraction across all grid cells. Note the log-scale on x-axis**

220

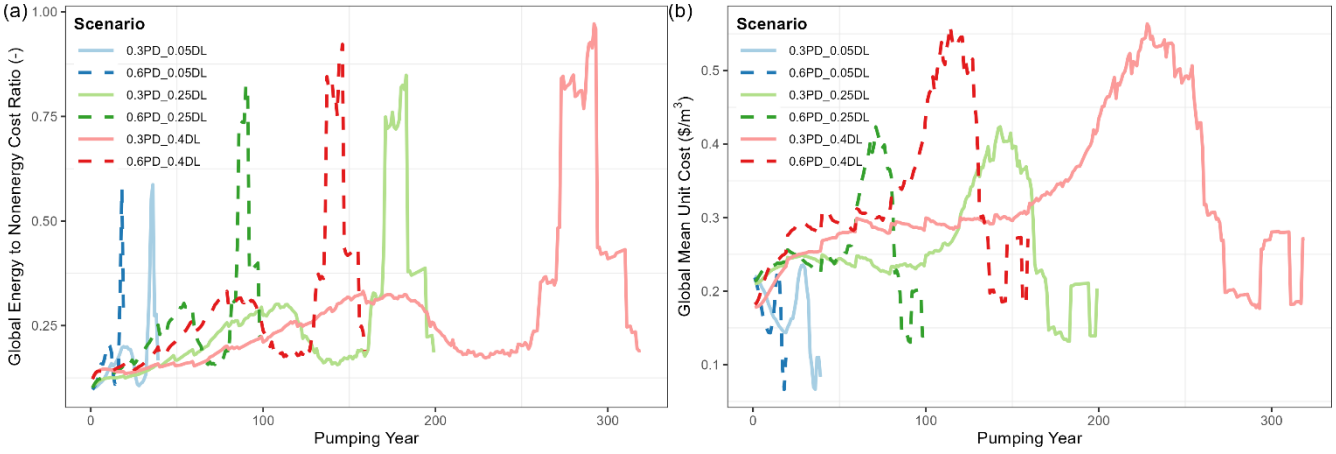

Fig. S39: Cost ratios: (a) Ratio of total energy costs to nonenergy costs ratio globally; and (b) Global mean unit cost (USD/m^3) calculated using a ratio of total cost of groundwater extraction over total volume extraction across all grid cells in a model pumping year, indicating the average cost of extracting a cubic meter of groundwater, in USD/m^3.

225

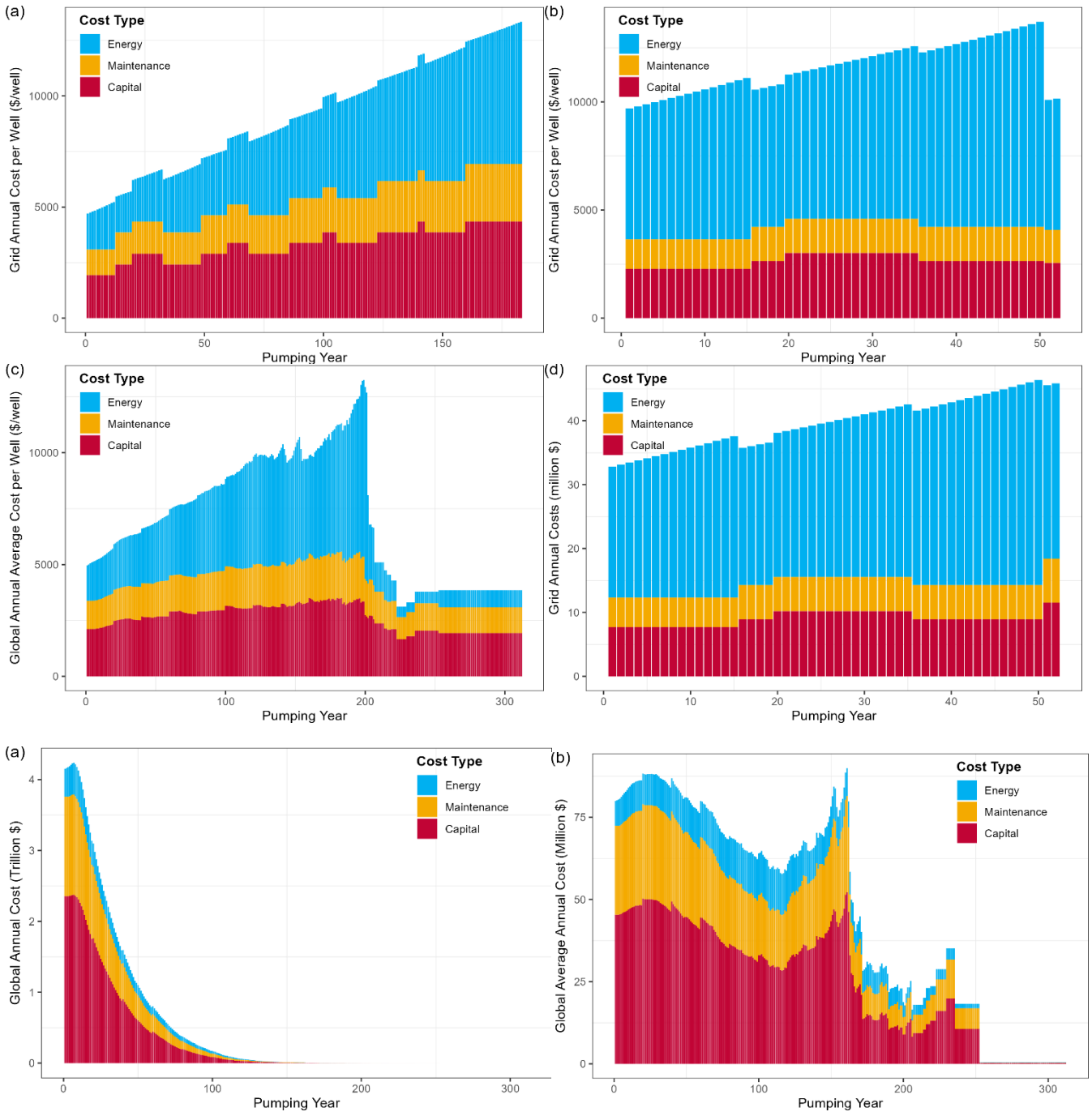

Fig. S40: All cost components stacked over each other for global (all grid cells) and a single grid cell.

S5 Details on Modelling Processes and Choices

S5.1 Lateral Flows

We have not modified the Theis equation or used image wells to represent no-flow boundaries between grid cells. While wells hypothetically located along the boundary of a cell could experience a larger amount of drawdown than wells within the interior of the grid cell, the overall effect given the pumping duration (100 days) and inverse relationship between well spacing and well pumping rate we impose (higher capacity wells are spaced further apart), results in negligible additional drawdown at wells that would be located near cell boundaries. Furthermore, the overall water balance of each grid cell is imposed at annual time steps where the total pumped volume from all wells is summed and converted into an equivalent decrease in saturated thickness across the entire grid cell. Incorporating natural recharge partially offsets the depletion from pumping and is also accounted for at the annual time scale.

S5.2 Sub-annual Pumping Duration

The 100-day assumption is based on upper bounds for annual average days of irrigation well pumping from US Department of Agriculture Farm and Ranch Irrigation Survey data (Fig. S41) (USDA, 2024). Bierkens et al. (2022) also use the assumption of 100 days of pumping for their global analysis of groundwater use for irrigation. Additionally, domestic wells or wells used for municipal supply are typically not operated 24 hours a day, 7 days a week so it seemed like a reasonable assumption to represent pumping for ~30% of the hours of the year. However, our analysis in Fig. S41 supports that bumping up the days of pumping to 150 days would not substantially adversely impact the assumption of recovery. The days of pumping can easily be adjusted in a .csv file outside of the model script and users could decide to evaluate different days of pumping either based on local information or as part of a sensitivity analysis.

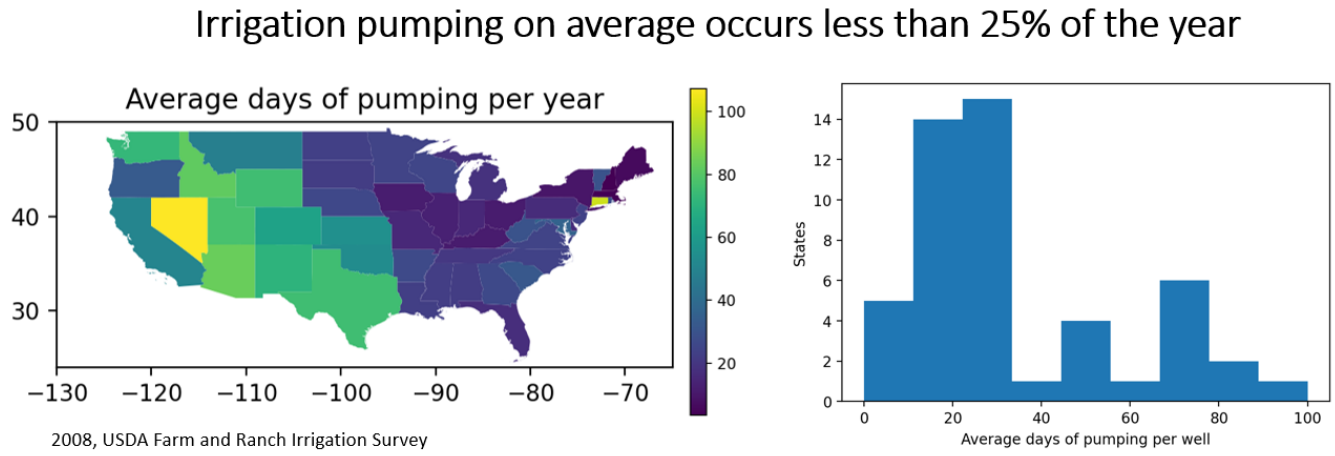

Fig. S41: Reported annual average days of irrigation well pumping by state in the continental United States (a) and the histogram of the annual average pumping data (b).

S5.3 Ponded Depth Targets

Ponded depth targets are exploratory variables (i.e., user-defined to explore pumping scenarios) that determine the annual pumping target. We modeled 0.3m and 0.6m keeping in view the crop water needs and effective root zone depth of major crops. These two values are supported by US Department of Agriculture data on annual average GW irrigation depths (Fig. S42b) (USDA, 2024). Based on this data, the 0.3 m value is a reasonable median value, while 0.6 m is a reasonable upper quartile value.

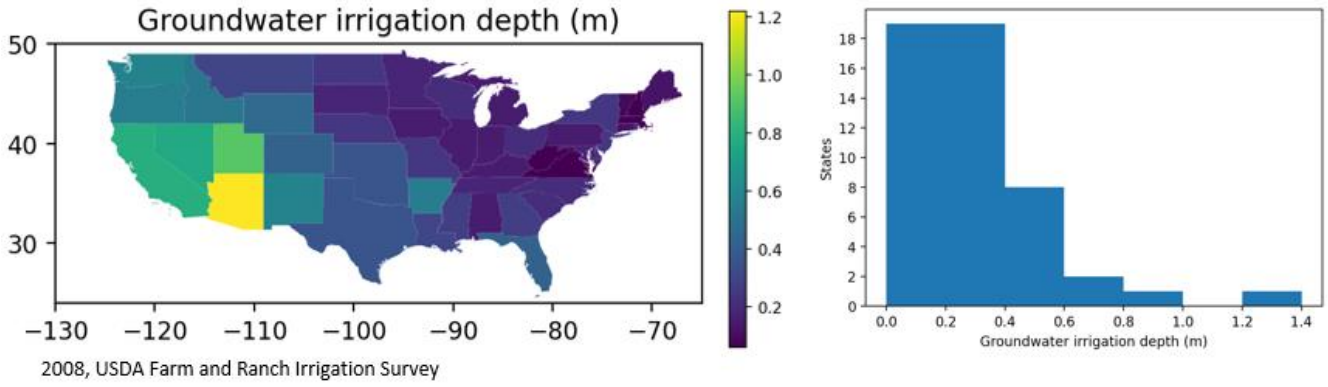

Fig. S42: Inferred irrigation depths (m/year) from US Department of Agriculture Irrigation Survey data mapped (a) and plotted as a histogram (b).

S5.4 Groundwater Head Recovery

Groundwater head recovery was not simulated using superposition in time by simulating an equivalent injection rate commencing at time = 100 days. We assume that the remaining 265 days allow the groundwater head to mostly re-equilibrate to an initial state. The validity of this assumption is supported by Theis modeling we performed using superposition in time to represent the head response at the well for scenarios of well pumping ceasing after 100 days and also for scenarios of 150 and 200 days of pumping (Fig. S43). The analysis presented is for a full-factorial sample (n = 735) across a wide range of potential hydrogeologic values with aquifer thickness of 50, 75, 100, 125 and 150 m, hydraulic conductivity K values of 0.1, 0.25, 0.5, 1, 2, 5, and 10 m/d, S_y values of 0.1, 0.2, 0.3, and pumping rates of 100, 200, 300, 400, 500, 600, and 700 gpm (Fig. S1 R1.4). Before plotting, the results were post-processed to filter out results that the violation check in Superwell would have screened as non-plausible and would have reduced the pumping rate before simulating pumping drawdown.

For the 100-day pumping scenario (Fig. S43), it can be seen that the head at the well location (r = 0.2 m) mostly recovers by day 365. We also plot maximum fraction drawdown versus recovery error (Fig. S39), which is the percent difference between full recovery being achieved by day 365 (i.e., returning to initial reference head of 0 m for this test case) and the final head value resulting from the pumping/injection superposition in time to represent pumping ceasing at day 100. The recovery error shows that the recovery error was less than 1% of saturated thickness, which supports that simulating the recovery is not necessary and that it is reasonable to assume full recovery at the end of each annual time step. At the end of each annual time step the depth to water is updated to reflect the grid cell level depletion (total pumping – recharge) and it is assumed the drawdown at each well has recovered. The results also show how the recovery assumption becomes less safe at longer durations of pumping and suggest that if 200 days were considered that it might be necessary to reduce the fractional drawdown limit to 0.3, which would keep the recovery error below 2%.

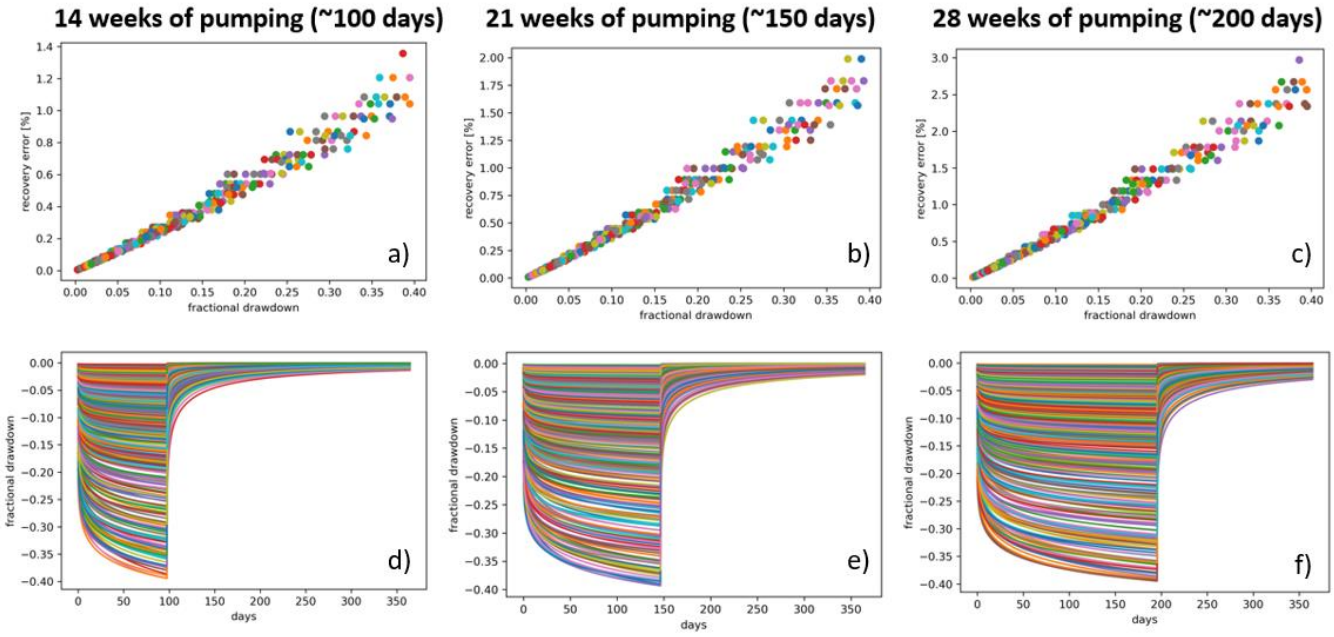

Fig. S43: Results for end of year head recovery for 100, 150, and 200 days of pumping (a-c), and corresponding fractional drawdown time series at the well (d-f).

S5.5 Well Deepening and Replacement

Well deepening and well replacements are standard adaptive responses of farmers to depleting aquifers and/or increasing water demands (Kyle et al., 2023). The choice of deepening 50m per every deepening instance is arbitrary. However, barring

a negligible number of edge cases where 50m deepening would be too much, it has no bearing on the unit cost estimates because if the initial 50m weren't enough the grid cell will deepen again in the following years to reach the pumping target.

S5.6 On Model Validation

Historical data in limited geographies and limited timespans could be used to validate the model, but it poses significant challenges. Structurally, the model is set up in a way to run such experiments by updating parameters in a .csv file outside the code of the model and utilizing the flexibility of the code to run based on the configuration specified by the user. However, doing such an exercise to replicate a region's pumping dynamics and associated costs will be highly constrained by the available data (Niazi et al., 2024c). For instance, validating for a small region will be conditional to data availability of not just hydrogeological properties, which we already use in Superwell, but also to gridded data of well properties such as well depths and pumping rates, farm areas served per well, etc., as well as the human choices and the cost data, including pumping rates, prevailing interest rates for financing, fuel prices, and labor and material costs for the installation of wells (Kyle et al., 2023; Zhang et al., 2024).

A major difficulty with region-specific historical validation would be in validating groundwater costs. In many cases in the U.S., the best available information from the United States Department of Agriculture (USDA) is the "pumping" cost for groundwater, which does not incorporate the infrastructure investments of drilling or maintaining the well. The USDA data is unique compared to the rest of the world in being openly available and easily accessed (USDA, 2024). Another aspect is if we were simply validating the depletion trends, that would mostly be a result of the water balance (the difference between total historical annual pumping timeseries and annual recharge timeseries) and not reflect well attributes or model representation.

In addition, one of the main purposes of the model is to produce cost curves, relating the unit cost of production and the volume produced. The top end of the cost curve (with the highest cumulative production and highest unit cost) could only be estimated in an exploratory way (Zhao et al., 2024), i.e., no region in our knowledge, with abundant data available for us to run a simulation, has reached the physical limits of groundwater extraction (i.e., run out of groundwater). In the absence of such extreme cases, full cost curves may not be validated even with historical data. In this study, we present Table B1 with unit cost estimates in Appendix B which shows Superwell cost estimates being in the range of previously reported unit costs of groundwater production from active groundwater supply aquifers.

In addition, the importance of exploring uncertainty can't be understated. We explore the uncertainty around varying depletion limits and pumping targets using a full factorial global sensitivity analysis of pumping targets and depletion limits. More discrete instances could be set up to explore the outcome space. Sensitivity analysis could be expanded to other variables such as interest rates, installation cost per unit of well depth, maintenance cost factor, well lifetime, and pump

efficiency, among others. The model is set up flexibly to ingest these parameters in a .csv file outside the code. A future improvement for us could be to make modifications to the model to improve the ease of setting up large experiments without manual launching of the simulations. Such simulations would help with more comprehensive sensitivity analysis to understand how model parameter assumptions and uncertainty in global datasets impact groundwater production and cost estimates and eventually human-Earth system outcomes in water supply, agriculture, municipal, and industry sectors (Kyle et al., 2023; Zhang et al., 2024; Zhao et al., 2024).

S6 Correlations

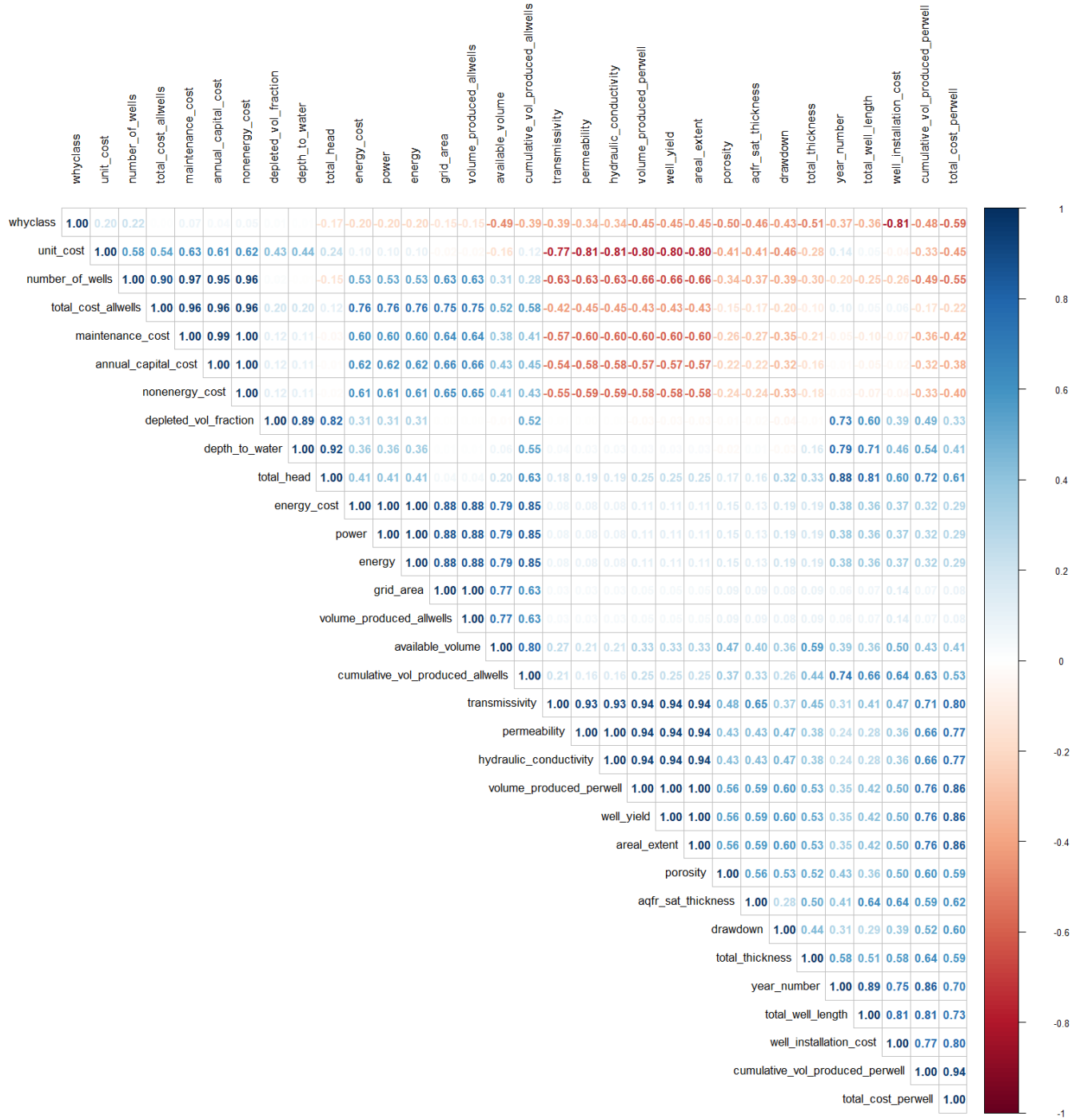

Fig. S44: Spearman correlation matrix of all inputs and outputs of superwell model (Niazi et al., 2024a; Niazi et al., 2024b)

S7 References

Bierkens, M., De Graaf, I. E., Lips, S., Perrone, D., Reinhard, A. S., Jasechko, S., van der Himst, T., and van Beek, R.: Global Economic Limits of Groundwater When Used as a Last Resort for Irrigation, https://doi.org/10.21203/rs.3.rs-1874539/v1, 2022.

Fan, Y., Li, H., and Miguez-Macho, G.: Global Patterns of Groundwater Table Depth, Science, 339, 940–943, https://doi.org/10.1126/science.1229881, 2013.

Gleeson, T., Moosdorf, N., Hartmann, J., and van Beek, L. P. H.: A glimpse beneath earth's surface: GLobal HYdrogeology MaPS (GLHYMPS) of permeability and porosity, Geophysical Research Letters, 41, 3891–3898, https://doi.org/10.1002/2014GL059856, 2014.

Kyle, P., Ollenburger, M., Zhang, X., Niazi, H., Durga, S., and Ou, Y.: Assessing Multi-Dimensional Impacts of Achieving Sustainability Goals by Projecting the Sustainable Agriculture Matrix Into the Future, Earth's Future, 11, e2022EF003 323, https://doi.org/10.1029/2022EF003323, 2023.

Messager, M. L., Lehner, B., Grill, G., Nedeva, I., and Schmitt, O.: Estimating the volume and age of water stored in global lakes using a geo-statistical approach, Nature Communications, 7, 13 603, https://doi.org/10.1038/ncomms13603, 2016.

Niazi, H., Ferencz, S., Yoon, J., Graham, N., Wild, T., Hejazi, M., Watson, D., and Vernon, C.: Globally Gridded Groundwater Extraction Volumes and Costs under Six Depletion and Ponded Depth Targets, https://doi.org/10.57931/2307832, 2024a.

Niazi, H., Watson, D., Hejazi, M., Yonkofski, C., Ferencz, S., Vernon, C., Graham, N., Wild, T., and Yoon, J.: Global Geo-processed Data of Aquifer Properties by 0.5° Grid, Country and Water Basins, https://doi.org/10.57931/2484226, 2024b.

Niazi, H., Wild, T. B., Turner, S. W. D., Graham, N. T., Hejazi, M., Msangi, S., Kim, S., Lamontagne, J. R., and Zhao, M.: Global peak water limit of future groundwater withdrawals, Nature Sustainability, 7, 413–422, https://doi.org/10.1038/s41893-024-01306-w, 2024c.

Niazi, H., Vernon, C., nkholod, and nealtg.: JGCRI/superwell: v1.1 (v1.1), https://doi.org/10.5281/zenodo.14583794, 2025.

Richts, A., Struckmeier, W. F., and Zaepke, M.: WHYMAP and the Groundwater Resources Map of the World 1:25,000,000, pp. 159–173, Springer Netherlands, Dordrecht, https://doi.org/10.1007/978-90-481-3426-7_10, 2011.

USDA, U. S. D. o. A.: Irrigation and Water Management, https://www.nass.usda.gov/Surveys/Guide_to_NASS_Surveys/Farm_and_Ranch_Irrigation/index.php, accessed: 2024-02-20, 2024.

Zhang, X., Sabo, R., Rosa, L., Niazi, H., Kyle, P., Byun, J. S., Wang, Y., Yan, X., Gu, B., and Davidson, E. A.: Nitrogen management during decarbonization, Nature Reviews Earth Environment, 5, 717–731, https://doi.org/10.1038/s43017-024-00586-2, 2024

Zhao, M., Wild, T. B., Graham, N. T., Kim, S. H., Binsted, M., Chowdhury, A. F. M. K., Msangi, S., Patel, P. L., Vernon, C. R., Niazi, H., Li, H. Y., and Abeshu, G. W.: GCAM–GLORY v1.0: Representing global reservoir water storage in a multi-sector human–Earth system model, Geosci. Model Dev., 17, 5587–5617, https://doi.org/10.5194/gmd-17-5587-2024, 2024.